Crack models of repeating earthquakes predict observed moment-recurrence scaling

C. Cattania[1,2], P.Segall[1]

[1]Department of Geophysics, Stanford University, Stanford, CA

[2]GFZ German Research Centre for Geosciences, Potsdam, Germany

Key Points:

- Analytical expressions for recurrence interval and stress drop of events on circular asperities in creeping faults
- Our models reproduce the observed scaling between recurrence interval and seismic moment of repeating earthquakes
- We predict and quantify a break in self similarity and decrease in stress drops close to the nucleation dimension

Corresponding author: Camilla Cattania, `camcat@stanford.edu`

Abstract

Small repeating earthquakes are thought to represent rupture of isolated asperities loaded by surrounding creep. The observed scaling between recurrence interval and seismic moment, $T_r \sim M^{1/6}$, contrasts with expectation assuming constant stress drop and no aseismic slip ($T_r \sim M^{1/3}$). Here we demonstrate that simple crack models of velocity-weakening asperities embedded in a velocity-strengthening fault predict the $M^{1/6}$ scaling; however, the mechanism depends on asperity radius, R. For small asperities ($R_\infty < R < 2R_\infty$, where R_∞ is the nucleation radius) numerical simulations with rate-state friction show interseismic creep penetrating inwards from the edge, with earthquakes nucleating in the center and rupturing the entire asperity. Creep penetration accounts for $\sim 25\%$ of the slip budget, the nucleation phase takes up a larger fraction of slip. Stress drop increases with increasing R; the lack of self-similarity due to the finite nucleation dimension.

For $2R_\infty < R \lesssim 4.3R_\infty$ simulations exhibit simple cycles with ruptures nucleating from the edge. Asperities with $R \gtrsim 4.3R_\infty$ exhibit complex cycles of partial and full ruptures. Here aseismic slip is less significant, and T_r is explained by an energy criterion: full rupture requires that the energy release rate everywhere on the asperity at least equals the fracture energy. This leads to the scaling $T_r \sim M^{1/6}$. Our results explain the occurrence of repeaters over a wide magnitude range, and the observation of events of different magnitude with overlapping rupture areas. We discuss observational constrains in each regime, in particular close to R_∞, and challenges with commonly used source models.

1 Introduction

Unlike large earthquakes, small quakes can be very predictable; periodic sequences of events with very similar waveforms have been detected in multiple locations worldwide. They are typically understood as the rupture of locked patches surrounded by aseismic creep loading them at a constant rate. An interesting observation is the scaling between their recurrence interval and seismic moment. *Nadeau and Johnson* [1998] observed that the recurrence interval T_r and seismic moment M_0 scale as $T \sim M_0^{1/6}$ for small repeaters on the San Andreas fault, and subsequent studies confirmed this scaling in other areas [*Chen et al.*, 2007]. As outlined by *Nadeau and Johnson* [1998], standard scaling arguments predict that $T_r \sim M_0^{1/3}$. Assuming constant stress drop constrains seismic slip to be linear with rupture dimension ($S \sim R$); further assuming that the coseismic slip is equal to the slip deficit accumulated since the previous event ($S = v_{pl}T_r$, where v_{pl} is fault slip rate) results in a linear scaling between recurrence interval T_r and R. Since $M_0 \sim \Delta\sigma R^3$ with constant stress drop $\Delta\sigma$, $T_r \sim M_0^{1/3}$. *Nadeau and Johnson* [1998] explained the observed scaling by abandoning the constant stress drop assumption, inferring $\Delta\sigma \sim M_0^{-1/4}$. To fit observations, very high stress drops (of the order of $10^3 - 10^4$ MPa) are required for the smallest events. Alternatively, the scaling can be explained by assuming constant $\Delta\sigma$ but relaxing the assumption that $S = v_{pl} T_r$, that is, by not assuming that the fault is entirely locked interseismically so that the coseismic slip is less than $v_{pl} T_r$. This was suggested by *Beeler et al.* [2001], who adopted a strain-hardening rheology on a circular patch experiencing spatially uniform interseismic creep. According to their model, smaller asperities release a large fraction of slip aseismically, which can result in the observed scaling. Similar conclusions were reached by *Chen and Lapusta* [2009], who presented numerical simulations of seismic cycles on circular, velocity-weakening asperities surrounded by a velocity strengthening exterior. They found that smaller asperities experience a larger fraction of aseismic slip, as suggested by *Beeler et al.* [2001]. Alternatively, *Sammis and Rice* [2001] proposed a geometrical explanation: asperities at the transition between locked and creeping regions experience a stress field decaying with distance from the transition, which under certain assumptions results in $T_r \sim M_0^{1/6}$. Because of the particular geometry, this may be less generally applicable than the aseismic slip interpretation.

Here we seek a deeper understanding of the factors that control the recurrence interval of earthquakes on circular asperities using fracture mechanics concepts, guided by numerical simulations of faults obeying rate-state friction, following *Chen and Lapusta* [2009]. The seismic moment of a circular crack of radius R with uniform stress drop $\Delta\sigma$ is [*Eshelby*, 1957]

$$M_0 = \frac{16}{7}\Delta\sigma R^3 \tag{1}$$

For constant stress drop, the scaling $T_r \sim M_0^{1/6}$ implies that $T_r \sim R^{1/2}$. Interestingly, this is analogous to the scaling derived by *Werner and Rubin* [2013] for antiplane faults loaded by downdip creep, by considering the balance between the energy release rate for a crack loaded by downdip creep and the fracture energy absorbed to propagate the crack through the full velocity weakening region. Here we demonstrate that, under certain assumptions, this energy argument applied to circular asperities leads to the analogous scaling for circular cracks. However, numerical simulations only exhibit this scaling above a critical radius (twice the nucleation radius R_∞, defined below), and that stress drop is not constant for asperities smaller than this dimension. We develop crack models to answer the following questions: (1) how long does it take for creep loading to nucleate a dynamic rupture? (2) once an event nucleates, under what conditions will it rupture the entire asperity? (3) how does stress drop vary with asperity dimension? We find that the answers to these questions depend on the asperity dimension R relative to R_∞. This is perhaps not surprising, since this dimension controls the transition between aseismic and seismic slip; the occurrence of creep affects the strength of the asperity and hence rupture propagation. Furthermore, as R approaches R_∞, the assumptions behind classical seismological models of circular ruptures break down: the rupture cannot be assumed to start at a point expanding subsequently to seismic rupture velocities. In this limit, the rupture is not self similar and the stress drop increases slightly with R. Combining these results, we obtain analytical estimates for the recurrence interval as a function of asperity radius R, which predict a scaling close to that observed in nature. In summary, we show that T_r scales approximately with $M_0^{1/6}$ over a range of asperity radii, however the underlying physics differs depending on asperity size.

2 Numerical simulations

In order to test the analytical results derived in the next section, we ran a set of simulations analogous to those presented by *Chen and Lapusta* [2009]: a circular velocity-weakening asperity on an otherwise velocity-strengthening planar fault. Here we use the pseudo-dynamic rupture code *FDRA* [*Segall and Bradley*, 2012; *Mavrommatis et al.*, 2017]

The frictional resistance on the fault τ_f is controlled by rate-state friction [*Dieterich*, 1978]:

$$\tau_f(v,\theta) = \sigma\left[f_0 + a\log\frac{v}{v_0} + b\log\frac{\theta v_0}{d_c}\right], \tag{2}$$

where σ is effective the normal stress; a, b and are constitutive parameters; d_c is the characteristic slip-weakening distance. v and v_0 are the slip velocity and a reference slip velocity; f_0 is the steady-state friction coefficient at $v = v_0$, and θ is a state-variable which here evolves according to the ageing law [*Ruina*, 1983]:

$$\frac{d\theta}{dt} = 1 - \frac{\theta v}{d_c}, \tag{3}$$

so that the steady-state strength at constant slip velocity v is given by

$$\tau_{ss}(v) = \sigma\left[f_0 + (a-b)\log\frac{v}{v_0}\right]. \tag{4}$$

Slip on the fault is controlled by the following equation of motion:

$$\tau_{el}(\mathbf{x}) - \tau_f(\mathbf{x}) = \frac{\mu'}{2c_s}v(\mathbf{x}), \tag{5}$$

where μ' is the shear modulus for antiplane shear and the shear modulus divided by $1-\nu$ (ν = Poisson's ratio) for plane strain deformation. τ_{el} is the elastostatic shear stress due to loading from the boundary and static elastic interactions between fault elements computed through a Boundary Element Method (BEM) approach. The right hand side represents radiation damping, which accounts for the stress change due to radiation of plane S-waves [*Rice*, 1993].

Rate-state friction combined with elasticity leads to characteristic dimensions which control earthquake nucleation, and the transition between seismic and aseismic behaviour. One such dimension is

$$L_b = \frac{\mu' d_c}{\sigma b}. \quad (6)$$

This length scale was first identified by *Dieterich* [1992] as the minimum nucleation length, although subsequent studies obtained different estimates [*Rubin and Ampuero*, 2005, and references therein]. We set $\mu = 30$ GPa, $\nu = 0.25$, $d_c = 0.1$ mm, $b = 0.02$ and $a - b = \pm 0.005$ for the velocity strengthening and weakening region respectively, resulting in $L_b = 4$ m (antiplane shear). We tested asperity radii R such that R/L_b is between 6 and 100. The system is driven by boundary velocity conditions $v = v_{pl}$ (10^{-9} m/s), and the domain size is $6R$ in each direction. As long as the domain boundaries are sufficiently far, the domain size has little influence of the simulation results: we tested sizes between $6R$ and $100R$ and found a variation of less than 1% in recurrence interval. We define earthquakes as the period during which the slip velocity at any point exceeds the threshold velocity $v_{dyn} = 2a\sigma/\mu' c_s$ (here 0.14 m/s) at which point the inertial term in Eq. 5 becomes significant [*Rubin and Ampuero*, 2005].

The rupture behaviour as a function or R is described in detail in *Chen and Lapusta* [2009]; here we sumarize the main results. The smallest faults ($R \leq 12.5 L_b$) are entirely aseismic. However, they also exhibit cycles: most slip takes place during short episodes of slip at a rate higher than loading rate (e.g. $v \sim 10^3\ v_{pl}$ for the smallest fault, $R = 6L_b$), and are nearly locked between such events. Intermediate size asperities ($15.7L_b \leq R \leq 20.5L_b$) exhibit cycles of seismic ruptures nucleating at the center of the asperity (Fig. 1). After each rupture, a creep front propagates inwards from the edge, and the next rupture occurs when the front reaches the center. There are no transient accelerations in slip velocity other than those leading to seismic rupture. For larger asperities ($R \geq 25L_b$) ruptures nucleate from the side, when the creep front has only partially penetrated the asperity. There are always one or more transient aseismic slip events in each cycle before reaching seismic velocities (Fig. 2). For $R \simeq 22L_b$, central and lateral ruptures alternate. Finally, we note that on the largest asperity tested ($R = 100L_b$) some seismic ruptures arrest before covering the entire asperity; we denote these as partial ruptures. As expected, our simulations result in the $T_r \sim M_0^{1/6}$ scaling observed by *Chen and Lapusta* [2009] (Fig. 3), across all the regimes of seismic ruptures described above.

However, Fig. 4 shows that the scaling between T_r and R varies with asperity radius. For seismic ruptures nucleating at the center, $T_r \sim R$; on asperities with lateral ruptures $T_r \sim R^{1/2}$ (consistent with $T_r \sim M_0^{1/6}$ scaling and constant stress drop). Aseismic events have shorter T_r compared to seismic central ruptures. In the following sections, we develop crack models to understand the scaling of T_r with R (section 4) and the variation of stress drop with asperity dimension (section 5).

3 Estimating $T_r(R)$ from crack models

We estimate the recurrence interval by treating aseismic and seismic slip on the asperity as cracks, and determine their propagation or arrest based on energy balance concepts [e.g. *Griffith*, 1921; *Freund*, 1990]. This approach is analogous to the estimation of the critical nucleation length by *Rubin and Ampuero* [2005] and to the estimation or recurrence interval on vertical antiplane faults by *Werner and Rubin* [2013]. As shown by *Irwin* [1957], these energy criteria can be expressed in terms of stress intensity factors (SIF). We consider the following contributions to the SIF, K: (1) K_l, the stress intensity factor of a stress-free crack subject to external loading (creeping surrounding the asperity); (2) $K_{\Delta\tau}$ the stress intensity factor due to changes in stress within the crack due to the variation in strength with slip velocity. A crack can grow if the total stress intensity factor is at least equal to the toughness K_c:

$$K_l + K_{\Delta\tau} \geq K_c, \tag{7}$$

where K_c is related to the fracture energy G_c by

$$K_c = \sqrt{2\mu' G_c} \tag{8}$$

following the convention of *Tada et al.* [2000]. We use this framework to model two phases of slip on the fault: the interseismic inward propagation of the creep front, and the propagation or arrest of a seismic rupture. Eq. 7 takes on two limiting cases: considering inward growth of the creeping zone, the slip speed immediately behind the crack tip is small (e.g. close to plate rate), thus the fracture energy, and hence K_c, is small, and $K_l \simeq -K_{\Delta\tau}$. On the other hand, considering seismic rupture into a region already at low stress, $K_{\Delta\tau}$ is small and Eq. 7 becomes $K_l \simeq K_c$ (the argument introduced by *Werner and Rubin* [2013] to estimate T_r for vertical antiplane faults). As shown below, these processes define two timescales: the time required for nucleation (T_{nucl}), and the time when a rupture can propagate over the full asperity (T_{full}).

4 Creep front propagation

4.1 Small asperities (central ruptures)

First we consider asperities small enough that the creep front reaches the center. Fig. 5(a,b) shows the propagation of the creep front for asperities of different sizes: Fig. 5 shows that the lines collapse to the same curve when both position and distance are normalized by a factor proportional to R. In appendix A , we estimate the equation of motion for the creep front by numerically solving Eq. 7 for an annular crack, with stress change given by the increase from a residual steady-state stress at coseismic slip speed $\tau_{ss}(v_{co})$ to steady-state friction at the fault slip-rate $\tau_{ss}(v_{pl})$, that is $\Delta\tau = \tau_{ss}(v_{pl}) - \tau_{ss}(v_{co})$ (see Fig. 5(c)). The black and dotted lines in Fig. 5(b) are the expected position of the front, with and without the contribution from fracture energy. Overall this model explains the creeping front propagation reasonably well, with a few differences: (1) early in the cycle, the creeping front propagates faster than expected, due to afterslip in the velocity strengthening region loading the fault faster than plate velocity; (2) towards the end of the cycle, the crack propagates faster than expected, due to stressing from the opposing creep front, while our model assumes creep at $v = v_{pl}$. In appendix A we find that, neglecting fracture energy, the time required for creep to reach the center and nucleate a rupture is

$$T_{nucl}(R) = \frac{4\Delta\tau R}{\pi\mu' v_{pl}} \equiv R/\dot{r}_c. \tag{9}$$

where we introduced the characteristic speed for the creep front propagation $\dot{r}_c = \pi\mu' v_{pl}/4\Delta\tau$. The numerical solution is close to the following expression (derived in appendix A):

$$a(t) = R\sqrt{1 - t\dot{r}_c/R} \tag{10}$$

where a is the distance of the crack from the center; eq. 10 is shown by the solid red line in Fig. 5. As the crack approaches the center, its propagation speed and slip velocity increase and eventually reaches v_{dyn}. It then expands outwards into the creeping region, where the stress is nearly uniform and equal to the steady state strength at v_{pl}, i.e., $\tau_{ss}(v_{pl})$. The stress intensity factor of an elliptical crack in a uniform stress field is an increasing function of its size [e.g. *Madariaga*, 1977]. Therefore, once nucleated the rupture accelerates and expands until it reaches the edge of the asperity: as seen in the simulations, all accelerating events on faults nucleating from the center result in full ruptures, so that in this regime the recurrence interval is determined by T_{nucl}. The linear trend in T_r vs. R (Figures 4 and 6) is in agreement with eq. 9. For even smaller (aseismic) asperities, we expect a similar behaviour, with v_{co} replaced by the slip speed during slow events. This speed, and hence $\Delta\tau$, decreases for smaller asperities, which explains why aseismic faults ($R/L_b < 12.5$) have shorter T_r than expected from eq. 9 calculated with $\Delta\tau = \tau_{ss}(v_{pl}) - \tau_{ss}(v_{co})$ for seismic slip speeds (Fig. 4).

4.2 Onset of lateral ruptures

As predicted by a linear stability analysis [*Ruina*, 1983], a creeping crack with velocity-weakening friction becomes unstable above a critical dimension (nucleation size), so that lateral ruptures occur on asperities with a radius exceeding some size. *Rubin and Ampuero* [2005] estimated a critical dimension for 1D cracks by treating the rupture as a constant stress drop crack with a stress intensity factor equal to the toughness determined from rate-state friction. Assuming steady state friction at seismic slip speeds immediately behind the crack tip, they estimate the maximum half-length for stable propagation to be:

$$L_\infty = \frac{1}{\pi}\left(\frac{b}{b-a}\right)^2 L_b \tag{11}$$

For a 2-D crack, we can assume that the rupture starts as a circular, penny-shaped crack within the creeping region of the asperity. For this geometry, we have $K_{\Delta\tau,p} = (2/\pi)\ K_{\Delta\tau,1D}$, where the subscripts p (penny) and $1D$ refer to the crack shape shape. The critical radius in 3 dimensions is thus:

$$R_\infty = \frac{\pi}{4}\left(\frac{b}{b-a}\right)^2 L_b \tag{12}$$

As in the analysis of [*Rubin and Ampuero*, 2005], this is an upper limit for the nucleation dimension, valid at large slip velocities (e.g. $v \gg v_{pl}$). Since instabilities start within the creeping annulus in the velocity weakening region (Fig. 2), instabilities can occur when the creep front has penetrated a distance $L_{pen} = 2R_\infty$. With the parameters used in our numerical simulations, $L_{pen} \sim 25L_b = 100$ m. If $R = 2R_\infty$ seismic rupture is expected to start at the center of the asperity, such that this length marks the transition between central and lateral ruptures, which in our simulations occurs at $R \simeq 22L_b = 88$ m, close to the $25L_b$ estimated. Furthermore, aseismic behaviour is expected for $R < R_\infty = 12.5L_b$. In our simulations, we find that the transition between aseismic and seismic slip occurs slightly above this value (between $R = 12.6\ L_b$ and $15.7\ L_b$; Fig. 6).

To estimate the time to nucleation since the last rupture, we make use of the equation of motion of the creep front derived in appendix A . Setting $a(t) = R{-}2R_\infty$ in eq. 10, and combining this result with eq. 9, we obtain the nucleation time:

$$T_{nucl} = \begin{cases} R/\dot{r}_c & R < 2R_\infty \\ 4R_\infty \left(1 - R_\infty/R\right)/\dot{r}_c & R \geq 2R_\infty \end{cases} \tag{13}$$

This is shown by the blue line in Fig. 6, which provides a close fit to the simulated recurrence times. For $R \gg R_\infty$, $T_{nucl} = 4R_\infty/\dot{r}_c$: the time to nucleation becomes independent of R. This is not surprising since this is approaching the 2D limit, when the creep front propagation is independent of R. However, it would be unphysical for the recurrence interval for events that rupture the entire asperity to be a constant above a certain source radius. To understand earthquake cycles for $R \geq 2R_\infty$, we need to consider the conditions that determine rupture evolution and arrest, discussed in the following section.

4.3 Rupture propagation and arrest for $R \geq 2R_\infty$

Ruptures nucleating laterally have to propagate through the locked part of the asperity ($r < R - 2R_\infty$). As they propagate towards the center, they encounter lower stresses (since the stress imparted by creep decreases with distance from the asperity edge: eq. A.5, fig. B.2). Therefore, ruptures may arrest within the locked region and not evolve into full ruptures; the recurrence interval, taken as the time between full ruptures, will be longer than T_{nucl}. We estimate the time between full ruptures by requiring that the minimum value of the SIF during rupture propagation balances K_c (the toughness associated with a crack slipping at coseismic speeds; e.g. *Werner and Rubin* [2013]). In appendix B we show that in this case Eq. 7 reduces to

$$K_l^* = K_c \tag{14}$$

where K_l^* is minimum value of the SIF associated with creep loading since the previous rupture. While an exact calculation of K_l^* requires knowing the shape of the crack as it evolves, dimensional arguments in appendix B lead to:

$$K_l^* = \frac{\mu' v_{pl}\ t}{\sqrt{R}}\ \phi, \tag{15}$$

where ϕ is a non-dimensional factor related to the shape of the rupture. The minimum time when full rupture is possible is therefore given by:

$$T_{full} = \frac{K_c}{\phi} \frac{\sqrt{R}}{\mu' v_{pl}}. \tag{16}$$

Assuming that the recurrence interval is close to T_{full}, we expect the scaling $T_r \sim \sqrt{R}$. This estimate of T_{full} ignores the influence of stress perturbations due to prior partial ruptures, and is therefore approximate. In order to estimate plausible values of T_{full}, in Appendix B we calculate ϕ numerically for a simplified rupture history, which gives $\phi = 0.76$. We point out that this value, and hence the minimum radius at which partial ruptures occur, is an order of magnitue estimate, since it greatly simplifies the shape and evolution of seismic ruptures.

We calculate K_c in eq. A.14 following *Rubin and Ampuero* [2005]. Due to healing, the fracture energy has a weak dependence on the time since the previous rupture. For the range of recurrence intervals considered, this has an effect of less then 10% on K_c, and for simplicity we set $\theta = 1$ year.

In appendix B.1 , we estimate that partial ruptures are energetically possible for $R \gtrsim 4.3R_\infty$: thus Eq. 16 applies above this value. In summary, we expect the recurrence interval to scale as $T_r = T_{nucl} \sim R$ on small asperities ($R < 2R_\infty$), and approximately as $T_r = T_{full} \sim \sqrt{R}$ on larger asperities ($R > 4.3R_\infty$), and with an intermediate exponent between the two (when $T_r \sim T_{nucl}$, but T_{nucl} scales sublinearly with R). This is broad agreement with numerical simulations (Fig. 6).

5 Stress drops and scaling between T_r and M_0

Crack models allow us to derive scaling relations between recurrence interval and source dimension. To understand the scaling with seismic moment ($M_0 \sim \mu\Delta\tau R^3$), we need to consider how stress drops scale with source radius. Fig. 7b shows how the seismic moment scales with R in the simulations. For the 5 smallest faults, an increase in stress drop with fault dimension is visible: this is due to a fraction of the seismic moment being released during the nucleation phase. Slip profiles during the seismic phase are well approximated by an elliptical crack with constant stress drop until the crack reaches the edge of the asperity, and by a circular, penny-shaped crack at the end of the earthquake. This predicts a constant stress drop during rupture growth, and also a constant stress drop for earthquakes of different size. However, fig. 7a shows that some of the slip is accumulates aseismically and thus does not contribute to the coseismic moment, defined as the moment released when $\geq v_{dyn}$.

As the crack expands, the slip velocity increases. The crack starts slipping at seismic velocities once it reaches a finite size (R_∞). We can then calculate the moment released during the nucleation phase from the moment of a penny-shaped crack of radius R_∞. The coseismic moment is then given by

$$M_0 = M_{0tot} - M_{aseis} = \frac{16}{7}\Delta\tau \left(R^3 - R_\infty^3\right) \tag{17}$$

where the first term is the total moment released from the beginning of nucleation phase to the end of the earthquake. The ratio between seismic and total moment is $1-(R_\infty/R)^3$ and it quickly approaches 1 (for example, almost 90% of the moment is released coseismically for $R = 2R_\infty$, which corresponds to the transition between central and lateral ruptures). This indicates that the variation in stress drops is only expected to occur over a limited range of fault dimensions.

From the simulations, we find that crack reaches $v = v_{dyn}$ when the semi-major and minor axes reach 55 m, 42 m respectively, in the inplane and antiplane directions, close to our estimate of R_∞ (50 m). As expected, this dimension is approximately constant with asperity dimension R (Fig. 7a). We estimate the total moment M_{0tot} directly from the slip profile: $M_{0tot} = \mu\pi S R^2/2$, where S is the slip at the center of the asperity. We find that the scaling of M_{0tot} from the simulations is consistent with self-similarity, as expected from the fact that the slip profiles in Fig. 7(a) have roughly the same shape. Furthermore, the scaling of M_0 with R is in agreement with eq. 17. For the smallest fault ($R \sim 1.3R_\infty$), the stress drop estimated from M_0 is about 50% smaller than the stress drop estimated from M_{0tot}.

Finally, we are in a position to combine the scaling of seismic moment with R and the dependence of T_{full} and T_{nucl} (eq. 16 and 13). This is shown in Fig. 8. While some slighty variations in the exponent are seen, we find that in the range $R_\infty < R < 4.33R_\infty$, the predicted trend is close to $T_r \sim M_0^{1/6}$. For $R \geq 4.33R_\infty$, we expect $T_r \sim M_0^{1/6}$ scaling from constant stress drop and $T_{full} \sim \sqrt{R}$. This is the central result of the paper.

5.1 Coseismic and interseismic slip budget

Figs. 9, 10 show the contribution of seismic and aseismic slip on asperities with different R/R_∞. Aseismic stress release occurs in various phases of the seismic cycle: (1) during the interseismic period, as a creeping front propagates inwards and part of the asperity slips at a speed of the order of v_{pl}; (2) during aseismic slip episodes such as those shown in Fig. 2; (3) during the acceleration and deceleration phase of an earthquake. The fraction of aseismic slip in phase (3) depends on the definition of “coseismic” slip velocity. The condition that the long-term slip rate on the asperity matches the loading rate can be expressed as follows:

$$S_{tot} = v_{pl}T_r = S_{seis} + S_{creep} + S_{nucl} + S_{post} \tag{18}$$

In Appendix C we derive analytical expressions for S_{creep} and S_{nucl} as a function of R/R_∞. Simulations do not exhibit significant postseismic slip within the velocity weakening asperity (Figs. 9, 10), consistent with results from spring slider simulations [*Rubin and Ampuero*, 2005; *Segall*, 2010] . We therefore neglect this process as well as the contribution of transient aseismic slip episodes and partial ruptures for $R > 4.3R_\infty$. Because of the latter assumption, these results are strictly valid only for $R < 4.3R_\infty$. Fig. 11a shows the values of S_{tot}, S_{creep} and S_{nucl} as a function of R/R_∞. As expected, S_{tot} has the same trend as T_r (Fig. 6). The slip from interseismic creep is also proportional to T_{nucl} for $R < R_\infty$ (asperities on which the creep front reaches the center); in Appendix C we show that $S_{creep}/S_{tot} = 0.25$. For larger values of R, interseismic creep is confined to part of the asperity $r > R - 2R_\infty$, and its contribution decreases with R. Finally, the fraction of slip during the nucleation phase decreases monotonically with R. Combining these results we estimate the ratio of seismic to total slip as

$$\frac{S_{seis}}{S_{tot}} = 1 - \frac{S_{as}}{S_{tot}} = 1 - \frac{S_{creep} + S_{nucl}}{S_{tot}} \tag{19}$$

shown in Fig. 11b. The ratio of seismic to aseismic slip derived from simple crack models provides a good fit to the trend the simulations.

6 Discussion

Based on energy balance arguments, and the scaling of stress intensity factors with asperity dimension, we identified the following regimes:

- $R < R_\infty$: asperities are aseismic.
- $R_\infty < R < 2\ R_\infty$, creep completely erodes the asperity and seismic rupture nucleate from the center. The recurrence interval scales as $T_r \sim R$. Stress drops increase weakly with R.
- $2\ R_\infty < R \lesssim 4.3\ R_\infty$: creep partially erodes the asperity before ruptures nucleate. When this occurs, the elastic energy accumulated from creep is sufficient for the rupture to propagate across the entire locked region, so that every nucleation results in a full rupture. The recurrence interval scales with $T_r \sim \sqrt{R}$.
- $R \gtrsim 4.3\ R_\infty$: the energy required for a rupture to propagate through the locked region exceeds the energy required for nucleation, and partial ruptures occur. The recurrence interval of full ruptures is expected to scale as $T_r \sim \sqrt{R}$.

Interestingly, we find that the scaling between seismic moment and recurrence interval is due to different physical reasons depending on R. For small asperities, the recurrence interval scales linearly with dimension; in this range of R, it is the increase of $\Delta\sigma$ with R that gives rise to $T_r \sim M_0^{1/6}$ scaling. The non-constant stress drop as R approaches the nucleation length is not surprising: crack models which predict constant $\Delta\tau$ assume a point source at $t = 0$, while the existence of a finite nucleation dimension breaks self-similarity as R approaches R_∞. For asperities with $R > 2\ R_\infty$, on the other hand, the relatinship between T_r and M_0 is dominated by the $T_r \sim \sqrt{R}$ scaling, which originates from the dependence of the stress intensity factor on asperity dimension. In other words, we recover the observed scaling by considering seismic ruptures as releasing accumulated elastic energy rather than stress.

A simplification in our crack models is the neglect of inertia when balancing the stress intensity factor and fracture toughness. While this assumption is valid for modeling creep propagation (and hence T_{nucl}), when applied to seismic ruptures it may lead to an underestimation of T_{full}. However, since inertial effects can be included by multiplying the SIF by a constant factor determined by the rupture velocity [*Freund*, 1990], we expect the $T_{full} \sim R^{1/2}$ scaling derived here to remain valid. Secondly, we note that a model of circular asperities with uniform frictional properties is extremely simplified: in nature, we expect some degree of stress heterogeneity due to fault roughness or variations in frictional and elastic properties, which would lead to more scatter in source properties and scaling. With this caveat in mind, below we discuss possible seismological observations predicted by our models.

6.1 Observations near the nucleation dimension

The existence of a finite nucleation dimension (R_∞) introduces a break in self similarity. While the value of R_∞ estimated here is specific to rate-state friction with certain parameters, we expect this result to be general: since the stiffness of a constant stress drop crack is inversely proportional to its size, slip on cracks below a critical dimension is aseismic [*Ruina*, 1983].

Could this variation in stress drop be observed in nature? The main difference between a numerical simulation and real earthquakes is that with simulations we know the asperity dimension. Therefore, when estimating stress drops, the larger fraction of slip released aseismically on smaller asperities leads to lower stress drops. However, the existence of a finite nucleation dimension also shortens the distance a rupture propagates before reaching the edge of the asperity. Asperity dimension is commonly estimated from the rupture duration, inferred from the corner frequency and assuming an expanding circular crack with constant rupture velocity [*Madariaga*, 1977; *Sato and Hirasawa*, 1973; *Kaneko and Shearer*, 2015]. For a rupture starting at $r = R_\infty$, the rupture duration will be shorter: in our simulations, it is proportional to $R - R\_\infty$. This may lead to underestimation of the asperity dimension as $R \to$

R_∞, and overestimation of the stress drops. To further complicate matters, the rupture velocity is not constant during this phase (since the crack is still accelerating). Therefore, smaller asperities have lower average rupture velocity, which may partially counteract the previous effect. These results indicate that assuming a circular source expanding at constant velocity may lead to large biases in the estimation of source properties at dimensions near R_∞. Finally, we point out that the definition of "earthquake" used here (based on a velocity threshold) probably does not accurately reflect the way seismic ruptures are recorded, making it difficult to directly translate our results into observable variations in source properties.

6.2 Transition between central and lateral ruptures

Circular sources propagating radially from the center are often used to infer source properties for small to moderate earthquakes. However, our results suggest that central ruptures only take place on asperities within a narrow range of dimensions ($R_\infty < R < 2_\infty$), and should therefore be quite rare for repeating earthquakes in nature.

Studies of rupture directivity for moderate to small events (down to about $M3.0$) indicate a prevalence of unilateral ruptures, and no variation with magnitude [*Boatwright*, 2007; *Abercrombie et al.*, 2017; *Calderoni et al.*, 2015]. A transition to central ruptures may occur at smaller magnitudes, for which estimating rupture directivity (or lack thereof) is particularly challenging.

6.3 Observations of partial ruptures

Finally, we estimated the minimum asperity radius that can host partial ruptures. While the exact dimension of the transition depends on the details of the asperity shape and assumptions in the derivation, the existence of such transition can be understood intuitively. Loading from the boundary of an asperity creates stress gradients within it, with lower stresses further away from the loading point. Stress increases everywhere with time, until an event can nucleate at the edge. If the asperity is large, the rupture will have to penetrate through a more extended region of lower stress, where it is more likely to arrest. This can also apply to other fault geometries: for example, *Werner and Rubin* [2013] and *Herrendorfer et al.* [2015] found a similar transition in 2-D models of subduction zones loaded by creep below the seismogenic zone. We demonstrated that the recurrence interval of full ruptures is expected to scale as $T_r \sim \sqrt{R}$, leading to the scaling observed in nature for repeating events: it is likely that most of the observed repeaters are in this regime. An interesting question is how the occurrence of partial ruptures may affect the degree of periodicity of the system. Partial ruptures introduce variability in the stress field, not considered in our derivation: for example, a rupture may arrest in the low stress region caused by a previous rupture [*Lapusta*, 2003], or be promoted by the stress concentrations outside its perimeter. These factors may affect not only the recurrence interval of full ruptures, but also their slip evolution and observed waveforms, practically determining an upper bound to the characteristic behaviour that defines a repeater. We note that the simulation with partial ruptures presents more variability in recurrence interval than those without (Fig. 4); however, due to computational costs this simulation only produces a small number of full ruptures (3), and we cannot draw strong conclusions. Further studies are needed to verify whether asperities above a certain dimension loose the periodicity and characteristic behaviour. Some indications of periodicity at large R/R_∞ can be inferred from the observed magnitude of repeaters, that can be as large as $M4.9{-}5.0$ [*Chen et al.*, 2009; *Uchida et al.*, 2012]. Combined with the observation that most events above $M3.0$ are unilateral, and therefore in the regime where $R > 2R_\infty$, this implies that asperities as large as $20R_\infty$ can have characteristic, quasiperiodic behaviour. An alternative plausible explanation for this magnitude range may be regional variation in R_∞. However, more direct evidence comes from the observation of multiple families of repeaters with overlapping rupture areas [*Uchida et al.*, 2007]: the $M4.9$ Kamaishi (Japan) repeater experiences interseismic partial ruptures, mostly located near its edge (as expected from the crack models presented here). Given that most of these partial ruptures are between $2 < M < 3$, the Kamaishi repeater appears to be an example of a periodic earthquake many times larger than R_∞.

6.4 Slip budget

Chen and Lapusta [2009] explained the scaling of T_r by the increase of seismic to aseismic slip ratio with R, as seen in Fig. 11; however, direct measurements of the slip partitioning at such small magnitudes have proven challenging. Using borehole strainmeter records of small events on the San Andreas fault, *Hawthorne et al.* [2016] observed that the fraction of postseismic slip doesn't vary significantly as a function of magnitude. Based on our models, we expect aseismic slip on the asperity to be taken up mainly during the interseismic and the nucleation phase. The propagation of the creep front on a circular fault is such that the creeping area grows approximately linearly with time (it would be exactly linear for the approximated equation of motion given by eq. 10); for a constant slip velocity behind the creep front, we thus expect a constant acceleration in moment. The total moment released by this process is not more than about a quarter of the total moment. The fractional contribution from the nucleation phase, on the other hand, can be arbitrarily large (Fig. 11).

7 Conclusions

We developed crack models of circular asperities embedded in a creeping fault, and found that they successfully reproduce the observed scaling between the recurrence interval and seismic moment: $T_r \sim M_0^{1/6}$. The temporal evolution of the creep front eroding an asperity is well fit by crack models, allowing us to quantify the contribution from aseismic slip during different phases of the seismic cycle.

Our models make specific prediction on the seismic behaviour of asperities as a function of the their dimension with respect to the nucleation radius R_∞. We identify a range of asperities over which ruptures nucleate from the center ($R_\infty < R < 2R_\infty$). Even though source models for events below $M5$ often assume central ruptures [e.g. *Boatwright*, 2007], we expect this behaviour to be relatively rare due to the narrow range of R. We also note that the existence of a finite nucleation size introduces a break in self-similarity, which results in a decrease of stress drop with R. This effect leads to the $T_r \sim M_0^{1/6}$ scaling for small asperities.

For larger asperities, the same scaling is not due to variations in stress drop but to the relationship between stress intensity factors and radius. In particular, we find that an energy balance argument predicts that full ruptures are possible at $T_{full} \sim \sqrt{R}$, and hence $T_r \sim M_0^{1/6}$. According to our analysis, this criterion explains the recurrence interval for asperities above $\sim 4.3R_\infty$. We discuss observational evidence suggesting that the largest observed repeater (the $M4.9$ Kamaishi, Japan repeater) falls into this regime.

Acknowledgements

C.C. was funded by a PRIME fellowship from the German Academic Exchange Service (DAAD) NSF award no. 1620496. We thank B. Ellsworth for helpful discussions. No data was used in this study.

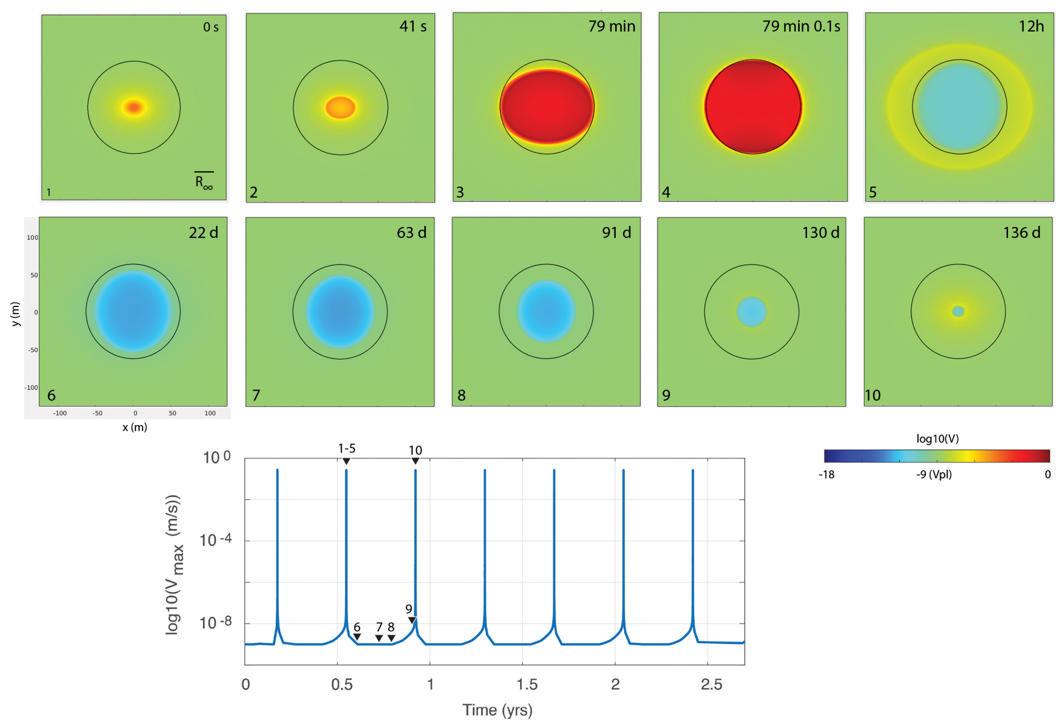

456 **Figure 1.** Top: full rupture on a fault of size $R = 16L_b$. Color is slip speed; slip is in the x direction. The time since the arrival of the creep front at $r = 0$ is indicated. Bottom: maximum slip velocity in the VW region vs. time, showing that this fault experiences periodic cycles of seismic ruptures. Numbers refer to the snapshots above.

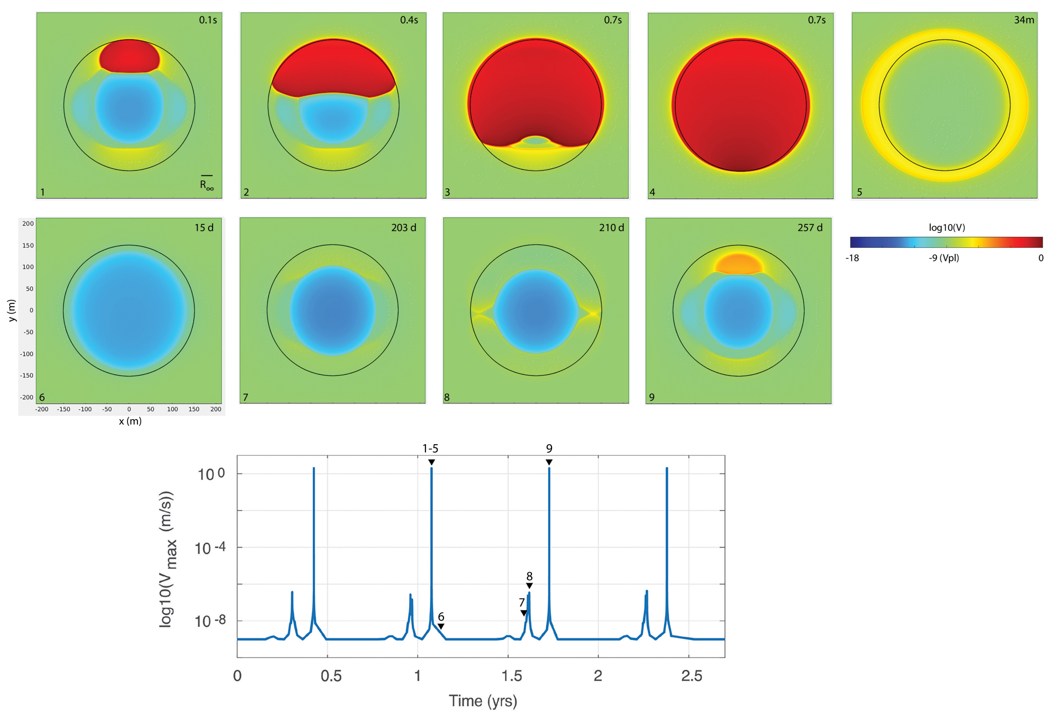

Figure 2. Example of a seismic cycles on a fault with $R = 38L_b$. Color is slip speed. Top: seismic event (panels 1-4) and afterslip (5). Inward propagation of a creep front, and a slip acceleration that does not reach seismic velocity (8). The time from the onset of the earthquake is indicated. Bottom: maximum slip velocity in the VW region vs. time, showing seismic and aseismic slip episodes. Numbers refer to the panels above.

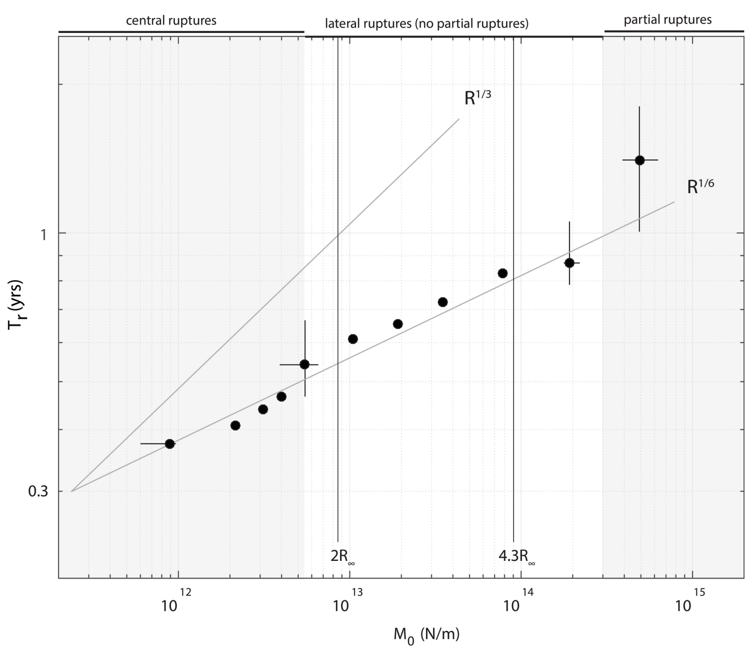

Figure 3. Scaling of T_r with seismic moment from numerical simulations. The y-axes is the time since the last rupture; we define T_r as the time between consecutive full ruptures. Error bars indicate range of observed T_r; the large variation for the fifth data point is due to the alternation of central and lateral ruptures.

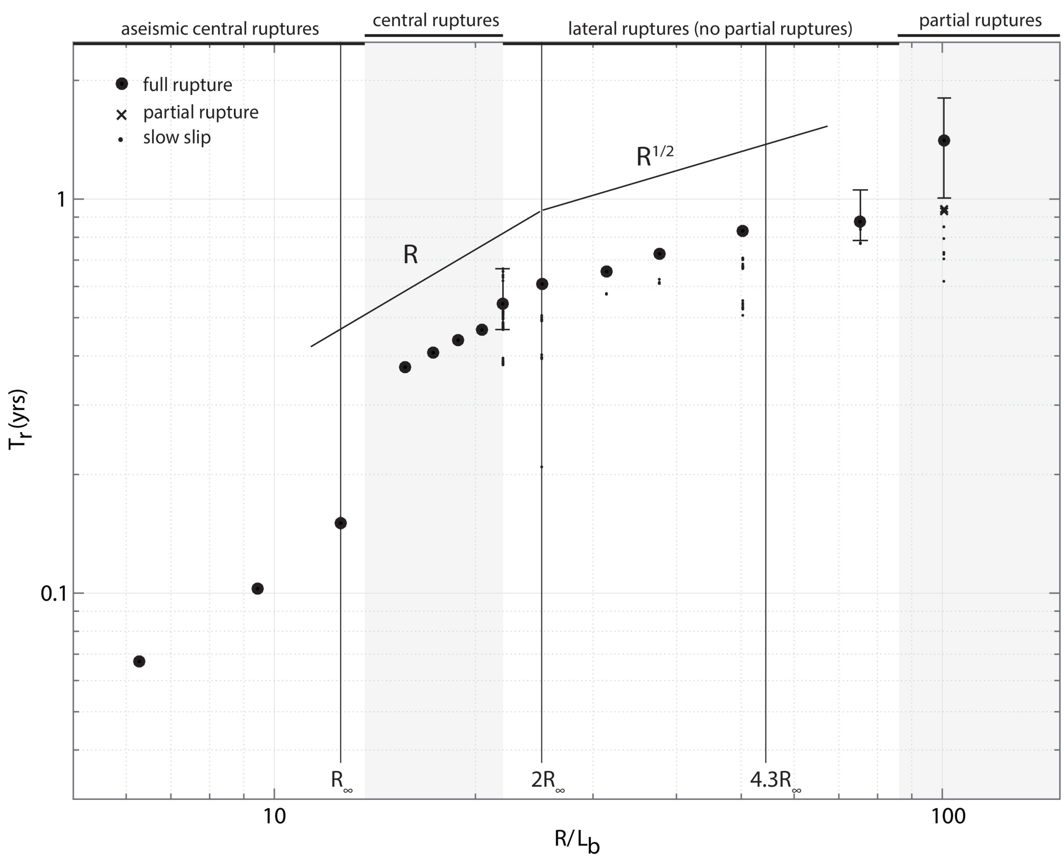

467 **Figure 4.** Scaling of T_r with asperity radius. For aseismic events, we define T_r as the time between peaks
468 in slip velocity. We denote "slow slip" brief slow slip events such as those in Fig. 2.

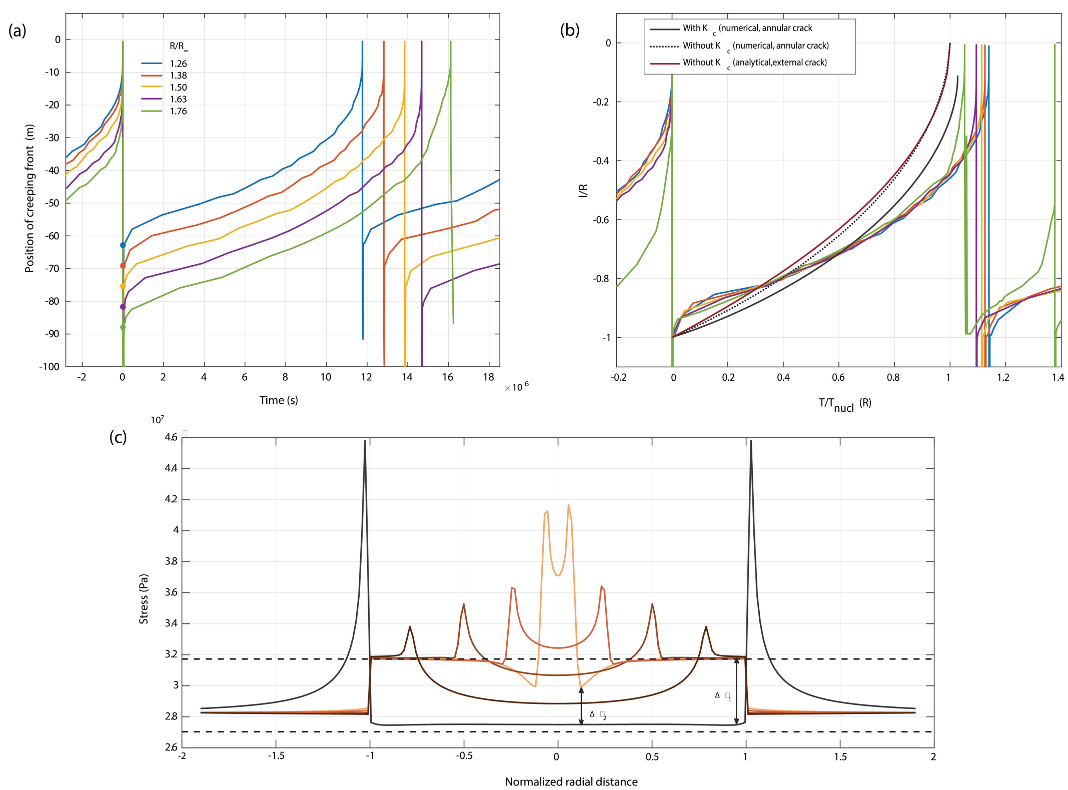

Figure 5. Top left: Interseismic propagation of creeping front from the edge of the asperity (indicated by the circle) to the center, estimated from peak stresses. The vertical lines are seismic ruptures. Top right: Same plot, with the y-axis normalized by asperity radius and the x-axis normalized Eq. 9. The black lines are the expected propagation of the front (see text). Bottom: stress profiles as the creep front propagates inwards. $\Delta\tau_1$ is the difference between residual stress after an earthquake ($\tau_{ss}(v_{co})$ and ($\tau_{ss}(v_{pl})$), shown by the dotted lines. As the creep front approaches $r = 0$, the slip velocity exceeds v_{pl} and the stress difference decreases ($\Delta\tau_2$).

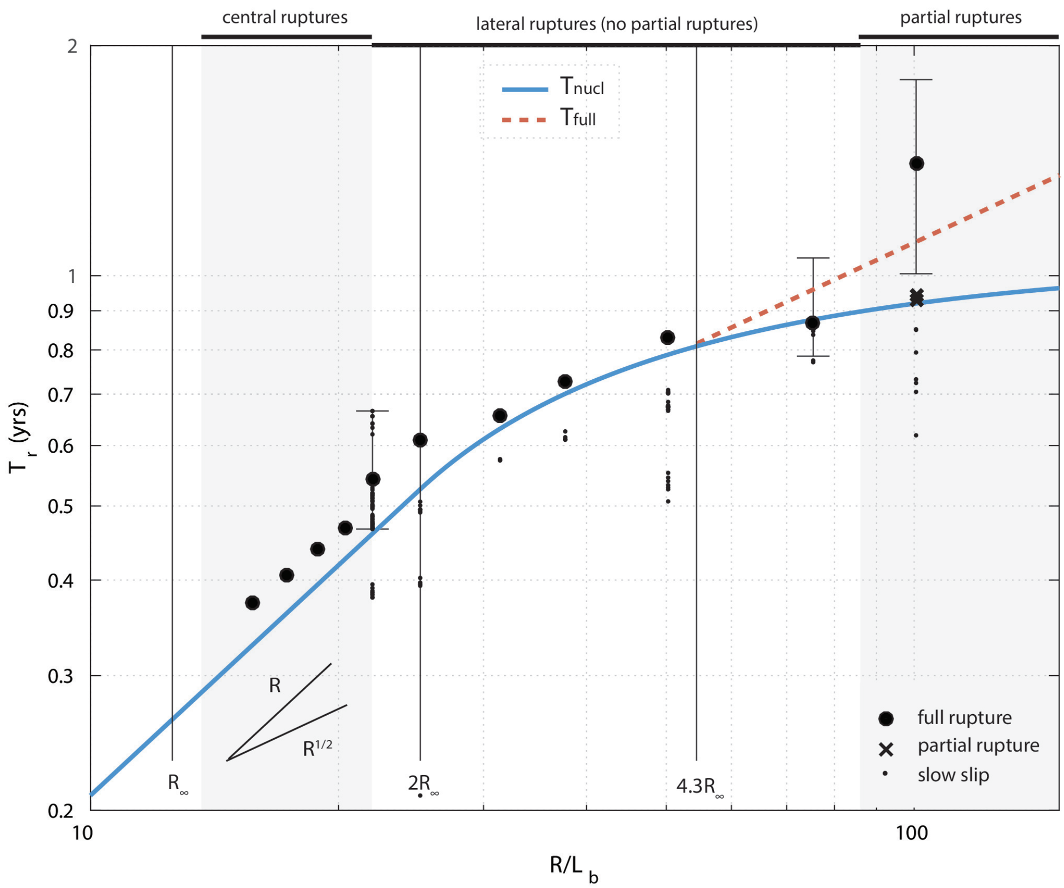

Figure 6. Scaling of T_r with R from the simulation (dots) and crack models (lines). Vertical lines mark the expected transition between regimes: aseismic to seismic (R_∞); central rupture to lateral ruptures ($2R_\infty$); onset of partial ruptures ($4.33R_\infty$), while the transitions observed in the simulations are marked at the top. T_{nucl} and T_{full} are calculated from eq. 13 and 16.

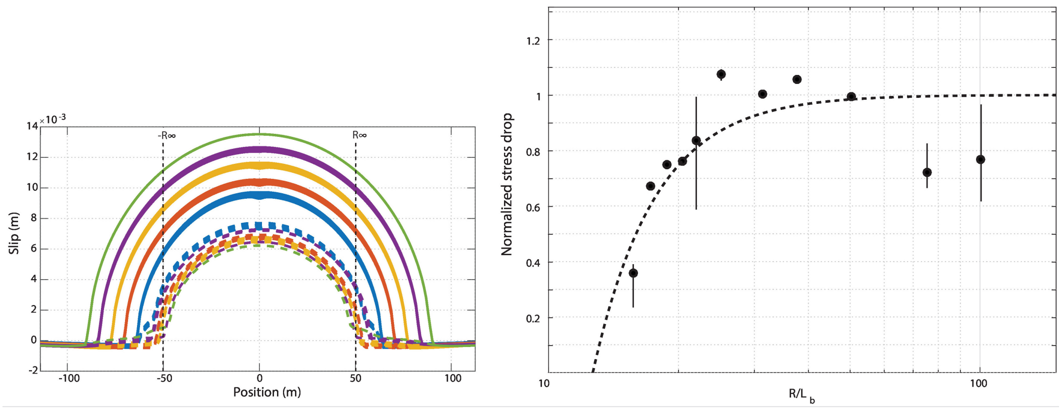

Figure 7. Left: slip profiles for central ruptures. Thick lines are the final slip distribution, dotted lines are the slip when the slip speed reaches v_{dyn} (i.e. at the start of an earthquake). Right: Stress drops in the simulations (dots) and expected from eq. 17, which takes into account the aseismic nucleation phase (dotted line). Stress drops are normalized by $\Delta\tau = 4.2$ MPa, which is the stress drop derived from the slip profile in the simulation and the expected limiting value as $R \gg R_\infty$.

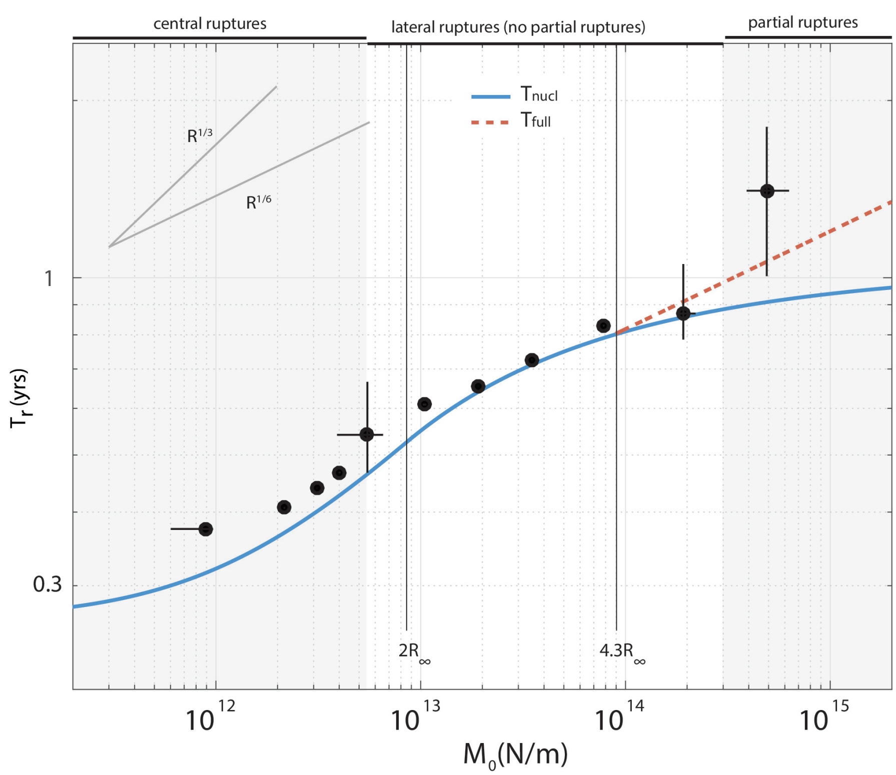

Figure 8. Scaling of T_r vs. M_0. T_{nucl} and T_{full} are from eq. 13, 16 and the seismic moment from eq. 17.

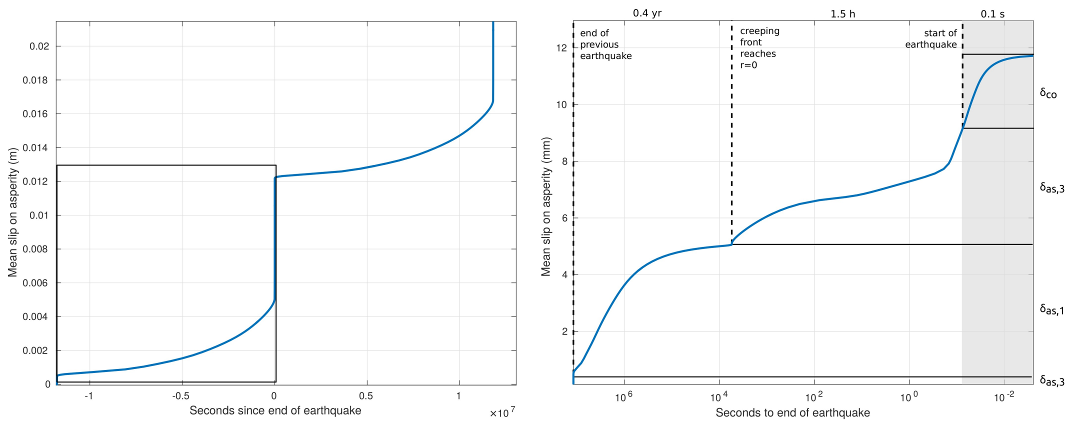

Figure 9. Average slip on the asperity during the cycle for the fault with $R = 16L_b$. δ_x are labeled as in Eq. 18.

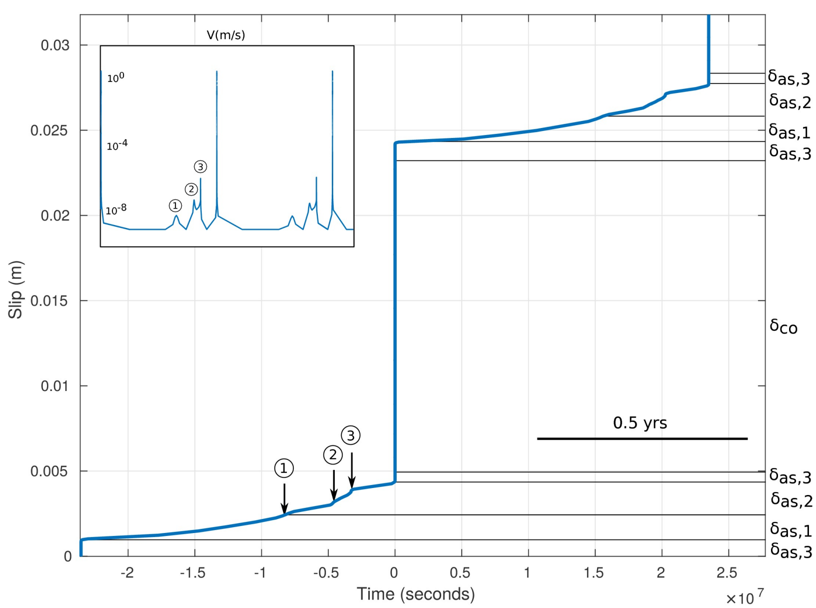

Figure 10. Average slip on the asperity during the cycle for the fault with $R = 50L_b$.

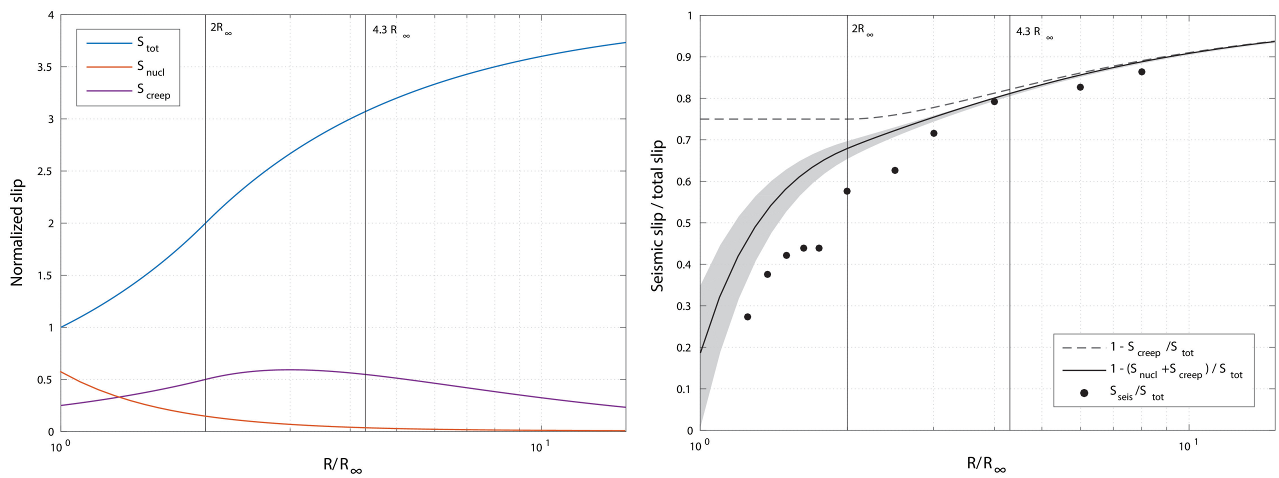

Figure 11. Left: slip budget estimated from eq. C.1, C.3 and C.4, normalized by the slip deficit on an asperity with $R = R_\infty$. Right: Fraction of seismic to total slip. Circles indicate the ratios observed in simulations; the black line is eq. 19, assuming that $\Delta\tau$ in eq. C.4 is the same as in eq. C.1, C.3. The grey area shows the range obtained allowing the stress drop during nucleation to differ from the stress increase during creep propagation ($\Delta\tau_{nucl} = [0.7 - 1.3]\Delta\tau_{creep}$).

A: Creep front propagation

In order to slip at the loading velocity, the stress behind the crack tip must increase from the residual stress after an earthquake $\tau_{ss}(v_{co})$ to the steady-state value at the creep rate $\tau_{ss}(v_{cr})$. In the simulations, we note that this is close to the loading rate v_{pl}, and for simplicity here we assume $v_{cr} = v_{pl}$. The crack can therefore be approximated by superimposing a stress-free end-driven crack and a crack with a spatially uniform negative stress drop $\Delta\tau = \tau_{ss}(v_{pl}) - \tau_{ss}(v_{co})$. Neglecting the contribution from fracture energy, the length of the crack $a(t)$ is determined by the condition that the total stress intensity factor vanishes, or

$$K_l(t, a) = K_{\Delta\tau}(a) \tag{A.1}$$

where K_l is the SIF due to displacement at $a \geq R$, which we assume to grow linearly in time ($S = v_{pl}t$). The propagating creep front can be treated as an annular crack driven by edge displacement, which grows in response to a increase in the displacement boundary condition (analogous to the 2-D case analyzed by *Mavrommatis et al.* [2017]). We consider an annular crack with outer radius R and inner radius $a(t)$.

A.1 Annular Crack

For simplicity, throughout this work we employ results for stress intensity factors for Mode-I cracks; for Mode-II or Mode-III cracks, the stress intensity factors vary by a factor of order 1. Closed form solutions for the stress intensity factors for an annular crack with fixed slip at $r = R$ are, to our knowledge, not available. Therefore we estimate them numerically, and validate these solutions by comparing them to analytical results in the limits: $a \ll R$ and $a \to R$. Consider an annular crack with inner and outer radii a and R, subject to an axisymmetric stress $\tau(r)$. The SIF can be expressed as

$$K(t, a) = \int_a^R \tau(t, r)k(r)dr \tag{A.2}$$

where $k(r)$ is the SIF for a unit ring force at radius r. We evaluate $k(r)$ numerically, using the method introduced by *Clements and Ang* [1988]. The stress distribution relevant for edge loading K_l is

$$\tau_l(r, t) = \tau_{rd}(r)\ v_{pl}t \tag{A.3}$$

where τ_{rd} is the stress due to a unit ring dislocation at $r = R$ (Fig. B.2), with slip $\delta(r, t)$:

$$\delta(r, t) = \begin{cases} v_{pl}t & r \geq R \\ 0 & r < R \end{cases} \tag{A.4}$$

where t is the time since the last event and v_{pl} the plate velocity. The stress field inside a dislocation ring is given by [*Kroupa*, 1960]:

$$\tau_{rd}(r) = \frac{\mu' v_{pl}\ t}{\pi R} \frac{E\left(\rho\right)}{1-\rho^2} \tag{A.5}$$

where $\rho = r/R$, and $E(k)$ is the complete elliptic integral of the second kind, which varies from 1 to $\pi/2$. It can be verified that this form gives the $1/x$ singularity in stress as $r \to R$ and reduces to $\tau_{rd} = \mu v_{pl} t/2R$ at $r = 0$. We checked that the numerical solution of $K_l(a)$, approaches known solutions for the two limiting cases: the result from *Selvadurai and Singh* [1986] for $a \ll R$, and the 2-D solution for $a \to R$.

For $K_{\Delta\tau}$, we assume a uniform (and negative) stress drop (Fig. 5), associated with increase in stress from that after dynamic rupture to steady state friction for creep at $v = v_{pl}$, i.e. $\Delta\tau = \tau_{ss}(v_{pl}) - \tau_{ss}(v_{co})$. We neglect the acceleration in slip speed (and hence decrease in $K_{\Delta\tau}$) as the slip front approaches the center (seen in the last snapshot in Fig. 5). We use the approximate solution from *Tada et al.* [2000]:

$$K_{\Delta\tau}(l) = \Delta\tau \sqrt{\frac{\pi l}{2}} \cdot F\left(\frac{l}{R}\right), \tag{A.6}$$

with

$$F\left(\frac{l}{R}\right) = \frac{1 - 0.36\ l/R - 0.067(l/R)^2}{\sqrt{1 - l/R}} \tag{A.7}$$

and $l = R - a$. Using our numerical solution for $K_l(t, a)$ (obtained through Eq. A.2 and A.5) and eq. A.6 into eq. A.1, we obtain the equation of motion for the creep front $a(t)$ shown in Fig. 5.

A.1.1 Calculating T_{nucl}

To get an analytical approximation for the time required for the creep front to reach the center of the asperity, we consider the limit $a/R \ll 1$. This is an estimate for the nucleation time on asperities with central ruptures. For K_l, we note that the stress intensity factor due to a displacement $\delta = S$ for $r \geq R$ and $\delta = 0$ for $r \leq a$ and zero stress in between is equivalent to that imposed by the boundary conditions $\delta = 0$ for $r \geq R$ and $\delta = -S$ for $r \leq a$, since the second state can be obtained from the first by subtracting a rigid body displacement, which generates no stresses. The stress field outside a dislocation ring of radius a and strength $-S = -v_{pl} T_{nucl}$ is [*Kroupa*, 1960]

$$\tau_{rd}(r) = \frac{\mu' S}{\pi a} \left[\frac{K\left(1/\rho\right)}{\rho} - \frac{\rho\ E\left(1/\rho\right)}{\rho^2 - 1} \right] \tag{A.8}$$

where $\rho = r/a$ and $K(k)$ is the complete elliptic integral of the first kind. As $1/\rho \to 0$, this becomes:

$$\tau_{rd} = -\frac{v_{pl}\mu'}{2a}\left(\frac{a}{r}\right)^3 T_{nucl} \tag{A.9}$$

for $r > a$. Since we are estimating the time for the creep front to reach the center of the asperity, $a(T_{nucl}) = 0$, we have $a/R \ll 1$ and can approximate the problem as an infinite external crack of radius a. Since the displacements at $r \to \infty$ for an external crack subject to a decaying field must be null, the boundary condition $\delta(R) = 0$ is automatically satisfied in this limit. The SIF for an external crack subject to a stress field of the form $\tau(r) = \tau_0(r/a)^{-n}$ (as in eq. A.9) is given by[*Sih*, 1973], and for $n = 3$ reduces to

$$K_l = -\frac{2}{\sqrt{\pi}}\tau_0\sqrt{a} = -\frac{v_{pl}\mu'}{\sqrt{\pi a}}T_{nucl} \tag{A.10}$$

The stress intensity factor for a constant stress drop (eq. A.6) in the limit $a/R \to 0$ is given by [*Tada et al.*, 2000]

$$K_{\Delta\tau} = \frac{4\Delta\tau R}{\pi^{3/2}}\sqrt{\frac{1-a/R}{a}} \sim \frac{4\Delta\tau R}{\pi^{3/2}\sqrt{a}} \tag{A.11}$$

Neglecting fracture energy, we set $K_l = K_{\Delta\tau}$ and obtain

$$t_0(R) = \frac{4R\Delta\tau}{\pi v_{pl}\mu'} \tag{A.12}$$

In the simulations, there is a delay between the arrival of the creep front and the onset of an earthquake; depending on R, this is of the order of seconds-hours (Fig. 1), and thus negligible compared to the cycle duration. Therefore we take the nucleation time T_{nucl} equal to t_0. We can gain some insight into how the asperity dimension affects creep front propagation by considering the scaling of K_l and $K_{\Delta\tau}$. Rewriting eq. A.10 in terms of the non-dimensional length $\tilde{a} = a/R$, we see that $K_l \sim t/\sqrt{R}$, a result which, as we demonstrate in Appendix B is valid for a crack of any shape within the asperity. Similarly, eq. A.6 shows that $K_{\Delta\tau} \sim \sqrt{R}$. Therefore, neglecting fracture energy and solving $K_l = K_{\Delta\tau}$ for a given value of $\tilde{a}$ results in $t \sim R$, so that when both distance and time are normalized by a factor proportional to R, the creep evolution curves collapes as in fig. 5. Fig. 5 also shows that the normalized equation of motion is in agreement with the equation of motion calculated numerically.

A.1.2 Effect of fracture energy

We include the effect of fracture energy by finding numerical solutions of

$$K_l + K_{\Delta\tau} = K_c \tag{A.13}$$

where K_c is the fracture toughness, which is related to the fracture energy by eq. 8. We employ the fracture energy for the aging law, in the no-healing approximation and constant slip velocity v_{in}, as given by [*Rubin and Ampuero*, 2005]:

$$G_c = \frac{d_c b\sigma}{2}\left[\log\left(\frac{v_{in}\theta_i}{d_c}\right)\right]^2 \tag{A.14}$$

Since the crack is propagating into the locked region, we take $\theta_i = t + d_c/v_{co}$ (from eq. 3, with $\dot{\theta} \sim 1$ and $\theta(t=0) = d_c/v_{co}$).

A.2 An approximate solution

Here we derive an analytical form for the equation of motion of the creep front by treating the annular crack as an external circular crack and approximating the stress field imposed by the ring dislocation at $r = R$. The SIF for an external crack of radius a subject to uniform stress between $r = a$ and $r = R$ is [*Sih*, 1973]:

$$K_{\Delta\tau} = \frac{2\sqrt{R}}{\sqrt{\pi}}\sqrt{\frac{1-\tilde{a}^2}{\tilde{a}}}\Delta\tau \tag{A.15}$$

with $\tilde{a} = a/R$. Note that this differs from Eq. A.11 due to the use of an external crack, as opposed to an annular crack. Next we approximate K_l as due to a concentrated ring force at $r = R$, i.e. $\tau(r) = P\delta(R)$, where P is a constant; $\delta(x)$ is the Dirac delta function, so that the ring force has the same form as the gradient of the imposed displacement (Eq. A.4). This approximation assumes that the SIF is dominated by the singularity in the stress field; we note that for 2 dimensional cracks, these two loading configurations produce exactly the same SIF ($K_l \sim \sqrt{l}$, where l is the distance between the loading point and the crack tip). The SIF in this case is *Sih* [1973]

$$K_l = \frac{2P}{\sqrt{\pi R}}\frac{1}{\sqrt{\tilde{a}(1-\tilde{a}^2)}} \tag{A.16}$$

Setting $P = \alpha v_{pl} t$ (so that K_l is proportional to load point displacement), $K_{\Delta\tau} = K_l$ gives

$$a(t) = R\sqrt{1 - \frac{\alpha v_{pl} t}{R}} \tag{A.17}$$

Further choosing $\alpha = \dot{r}_c/v_{pl}$ with $\dot{r}_c = \pi\mu' v_{pl}/4\Delta\tau$ matches the condition given by eq. A.12. This solution, although not rigorous, is close to the numerical result (Fig. 5).

B: Estimating $T_{full}(R)$

Eq. 7 considers the contribution of energy from elastic loading (K_l) as well as stress variations within the crack ($K_{\Delta\tau}$). In appendix A , we saw that the propagation of the creep front is controlled by both terms. For a seismic rupture, the problem can be simplified by noting that we are considering a full seismic cycle, so that the net stress change is null. At $t = 0$ (just after a full rupture) the stress in the asperity is low: $\tau = \tau_{ss}(v_{co})$. Interseimically, creep outside the asperity raises the applied stress, while frictional strength changes as a result of healing as well as creeping on part of the asperity. These interseismic stress changes are reversed during seismic rupture, since the stress behind the seismic crack tip is $\tau = \tau_{ss}(v_{co})$. Therefore we can set $K_{\Delta\tau} = 0$. For this argument to be strictly valid, we should define the crack as not only the seismic rupture, but the total slip accumulated interseismically. However, for simplicity, here we neglect the contribution from interseismic slip and assume that the asperity is entirely locked (a good approximation for $R \gg R_\infty$).

We estimate the stress intensity factor for a rupture nucleating at the edge of an asperity and propagating into the locked region. For a rupture in 2 dimensions, the stress intensity factor is a function of position along the front and it changes as the rupture grows. We consider the problem of a crack of an arbitrary shape growing within an asperity.

Rice [1989] developed a theory for calculating stress intensity factors for 2-dimensional cracks in a 3-D medium. For a crack subject to a stress field $\sigma(\mathbf{x})$, the stress intensity factor at position s along the rupture front is given by

$$K_l(s) = \int_{crack} k(\mathbf{x}; s)\sigma(\mathbf{x})dA \tag{B.1}$$

with

$$k(\mathbf{x}; s) = \frac{\sqrt{2\rho(\mathbf{x})}W(\mathbf{x}; s)}{\sqrt{\pi^3}D^2(\mathbf{x}; s)} \tag{B.2}$$

where ρ is the minimum distance between $\mathbf{x}$ and the edge of the crack, D the distance between $\mathbf{x}$ and point s along the crack, and $W(\rho, D)$ a non-dimensional factor which takes into account the crack shape (see Fig. B.1). The terms $k(\mathbf{x}; s)$ are weight functions: they depend on the crack geometry and not on the applied stress. Note that they are a function of position along the front, and they vary as the rupture grows and potentially changes shape. The applied stress field $\sigma(\mathbf{x})$ is determined by the loading conditions on the asperity (i.e. interseismic loading), and is given by eq. A.5. We can now write the stress intensity factor in terms of non-dimensional variables $\xi = r/R$, $\tilde{\rho} \equiv \rho/R$ and $\tilde{D} \equiv D/R$:

$$K_l(s) = \frac{\mu' v_{pl}\ t}{\sqrt{R}}\ \phi(s) \tag{B.3}$$

with

$$\phi(s) = \int \frac{\sqrt{2\tilde{\rho}(\mathbf{x})}W(\mathbf{x}; s)}{\sqrt{\pi^5}\tilde{D}(\mathbf{x}; s)^2}\frac{E(\xi)}{1-\xi^2}d\tilde{A} \tag{B.4}$$

Where the integration is over the rescaled crack. Note that this term only depends on normalized lengths. As the crack grows and changes shape, the quantities and $\tilde{\rho}$, $\tilde{D}$ and W vary. A rupture stops when $K_l(s) < K_c$ for all points s which are still within the velocity weakening region (or after penetrating a short distance into the VS region). For easier notation, we drop the dependence on s and we simply write $K_l < K_c$ when referring to this condition.
A first order scaling between the stress intensity factor and the asperity size can be derived by assuming that ϕ does not depend on R. This implies that rupture evolution is independent of asperity dimension, i.e. the rupture history on an asperity is simply a rescaled version of the rupture history on an asperity of a different size. This can be considered an acceptable first-order approximation given that $\tilde{\rho}$, $\tilde{D}$ must always be in the range $[0, 2]$. By setting Eq. B.3 equal to K_c we obtain an estimate of the minimum recurrence interval:

$$T_{full} = \frac{K_c}{\phi} \frac{\sqrt{R}}{\mu' v_{pl}} \tag{B.5}$$

and with constant ϕ we find a square-root scaling between recurrence interval and source dimension.

To estimate realistic values of $T_{full}(R)$, we compute ϕ numerically for the rupture history shown in Fig. B.2, using the values of $W(\mathbf{x}; s)$ for an elliptical crack [*Wang et al.*, 1998]. In this case K varies along the rupture front. For the innermost point along the rupture front (P), we note that the ϕ has a non-monotonic behavior as the rupture dimension grows: as P moves towards the center of the asperity, the stress field near P decreases and so does $\phi(P)$. Note that the minimum of K occurs before P reaches the center of the asperity, since $\phi(P)$ does not depend only on the stress at P but also on the crack size (it increases with crack dimension). The minimum value of ϕ is 0.76.

The behavior of stress intensity factor at one point is not enough to determine whether the rupture stops. However, this simple model shows that ruptures starting at the edge of an asperity and propagating down a stress gradient may encounter a minimum SIF as they grow. This may lead to either partial seismic ruptures, or slow slip episodes, depending on whether the minimum is encountered before or after reaching the critical nucleation dimension.

B.1 Transition to partial ruptures

Numerical simulations indicate that partial ruptures only occur for asperities above a certain size. The occurrence of partial ruptures can be understood in terms of the criteria described above: if the time of the first nucleation (Eq. 13) is smaller than T_{full}, partial ruptures will

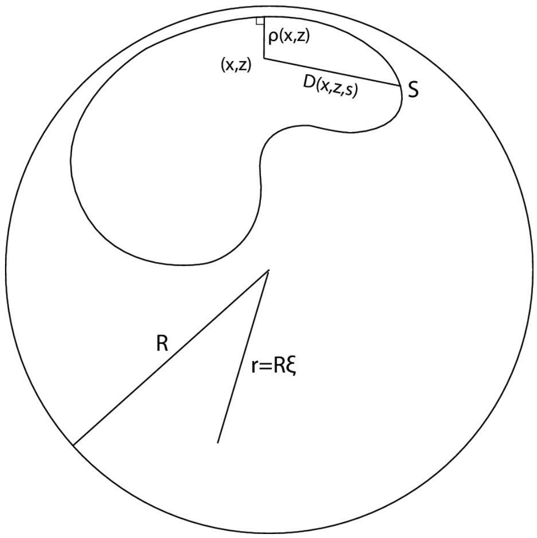

Figure B.1. Example of a rupture propagating within the asperity, as presented in *Rice* [1989]. The dimensions relevant to the calculation of stress intensity factors (Eq. B.2) are marked.

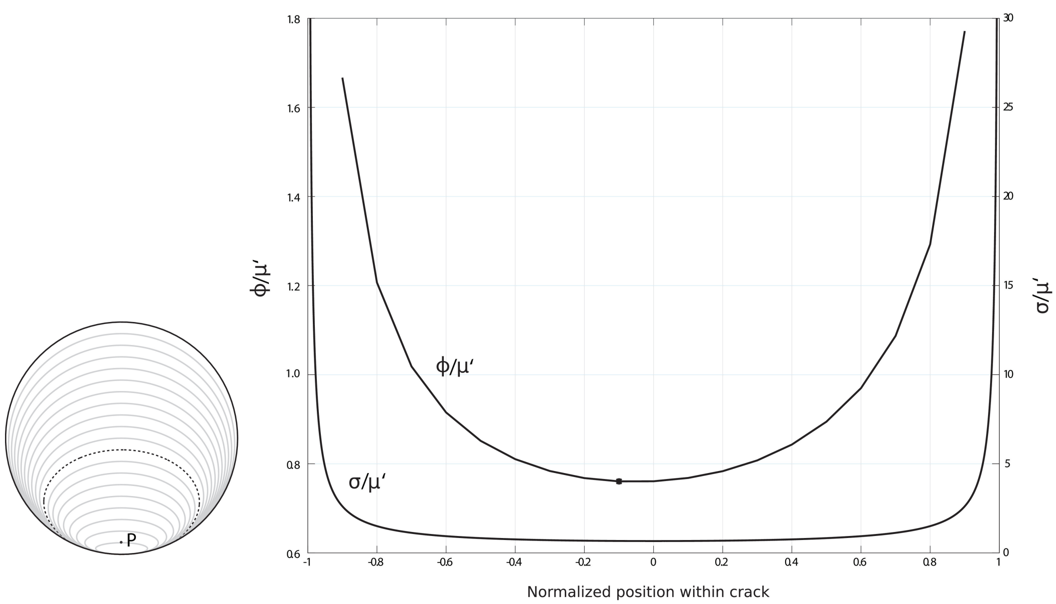

Figure B.2. Stress intensity factor for a rupture nucleating on the side. Left: sequence of elliptical cracks representing an idealized rupture history. Each ellipse is obtained by shifting the center along the vertical and matching the asperity curvature at the point of contact. Right: Stress intensity factor and stress field within the asperity. The stress intensity factor is calculated at point P (left panel). The minimum in ϕ (0.76) is marked with a circle, and it corresponds to the dotted ellipse in the left panel.

occur. While we could obtain the transition directly comparing these values, here we present a more general approach that can in principle be extended to different loading geometries. The main result is that the occurrence of partial ruptures is controlled primarily by the asperity geometry (shape and size); and to a smaller degree, by the value of the state variable in creeping vs. locked parts of the asperity. Notably, none of the frictional parameters, except d_c, appear in the final expression.

We estimate the value of R corresponding to a transition to partial ruptures by comparing the energy available at the time of nucleation with the energy required for a rupture to propagate across the entire asperity; fig. B.3(a) summarizes the criteria for creep propagation, rupture initiation and rupture propagation. The criteria for rupture nucleation and rupture propagation can both be expressed in the form $K_l = K_c(\theta_i)$, where K_l is the SIF associated with loading from creep in the VS region, and $K_c(\theta_i)$ is the toughness. Note that K_c depends on the value of the state variable in front of the crack tip θ_i, which is different depending on whether the rupture propagates through the creeping or locked part of the asperity. The terms K_l also differ between nucleation and rupture propagation, due to different crack geometry. The critical condition for full rupture is

$$\frac{K_l^*}{K_c(\theta_{lo})} = 1 \tag{B.6}$$

Here K_l^* denotes the minimum value during rupture propagation (see previous section), and $K_c(\theta_{lo})$ is the fracture energy as the crack propagates through the locked region. The nucleation length derived in section 4.2 for dynamic ruptures within an annular region can be derived from the criterion that the stress intensity equal the local fracture toughness:

$$K_{\Delta\tau,p} = K_c(\theta_{cr}), \tag{B.7}$$

where $K_c(\theta_{cr})$ is the fracture energy for a crack in the creeping region. The subscript p (penny) refers to the shape of the nucleating patch. We estimate values for the rock toughness in the two cases by taking $\theta = d_c/v_{pl}$ in the creeping region and $\theta = t$ in the locked region. From eq. A.14 we see that their ratio is

$$\frac{K_c(\theta_{cr})}{K_c(\theta_{lo})} = \frac{\log(v_{co}/v_{pl})}{\log(v_{co}t/d_c)}. \tag{B.8}$$

As discussed, $K_c(\theta_{lo})$ depends weakly on time, and we assume $t = 1$ year as a representative value for the recurrence interval, which yields $K_c(\theta_{cr})/K_c(\theta_{lo}) = 0.8$. For a recurrence interval of 1 day and 100 years, the ratio is between 1.0 and 0.7.

We can relate the nucleation condition to the loading from creeping in the VS region by noting that the condition controlling creep front propagation (section 4) is

$$K_{l,a} = K_{\Delta\tau,a} \tag{B.9}$$

where the subscript a (annulus) refer to the creep front geometries (see Fig. B.3). Now we can write

$$K_{l,a} = \frac{K_{\Delta\tau,a}}{K_{\Delta\tau,p}}\ K_c(\theta_{cr}) \tag{B.10}$$

The stress drops in eq. B.7 and B.9 have the same absolute value: for $K_{\Delta\tau,p}$, the stress is lowered from steady-state strength at plate rate to steady state strength at seismic velocities; for $K_{\Delta\tau,a}$ the change in stress is equal and opposite. Therefore, eq. B.10 expresses the nucleation condition in terms of loading and the geometrical factor $K_{\Delta\tau,a}/K_{\Delta\tau,p}$ depending only on R/R_∞ (black line in Fig. B.3(b)). Similarly, the SIFs due to loading (K_l^* and $K_{l,a}$) are both proportional to the slip outside the asperity, and their ratio is determined by geometry alone; Fig. B.3(c) shows how this ratio varies with R/R_∞, with K_l^* estimated setting $\phi = 0.76$ in eq. 15. Intuitively, when a rupture nucleates on a small asperity, it can easily evolve into a full rupture: by the time $K_{l,a}$ is large enough for rupture nucleation, K_l^* is also sufficient for the rupture to propagate through the asperity. On the other hand, for larger R/R_∞, a rupture may stop as it propagates within the locked region ($r < R - 2R_\infty$), since in this case the criterion for full rupture is more stringent than the criterion for nucleation.

More quantitatively, we combine B.6 and B.10 to give

$$\frac{K_l^*}{K_c(\theta_{lo})} = \frac{K_l^*}{K_{l,a}}\ \frac{K_{\Delta\tau,a}}{K_{\Delta\tau,p}}\ \frac{K_c(\theta_{cr})}{K_c(\theta_{lo})} \tag{B.11}$$

Since the first two fractions in eq. B.11 are controlled by geometry alone, this notation allows to check whether the criterion for full rupture is satisfied at the time of the first nucleation, only based on the value of R/R_∞ and the ratio $\frac{K_c(\theta_{cr})}{K_c(\theta_{lo})}$. From Eq. A.14 we note that, for a fixed slip velocity inside the crack, this term depends only on θ and d_c, while all other rate-state parameters cancel out. Fig. B.3(d) shows the ratio $K_l^*/K_c(\theta_{lo})$: for $R \gtrsim 4.3R_\infty$, we find that $K_l^*/K_c(\theta_{lo}) < 1$, so that partial ruptures can occur. In our simulations, we see partial ruptures starting slightly above this value (Fig. 6). From Fig. B.3(d), we see that $K_l^*/K_c(\theta_{lo}) < 1$ also occurs for $R \lesssim 0.8\ 2R_\infty$. However, in this case we do not see partial ruptures; this is most likely because most of the asperity is creeping, while K_l^* was estimated assuming propagation in a locked asperity.

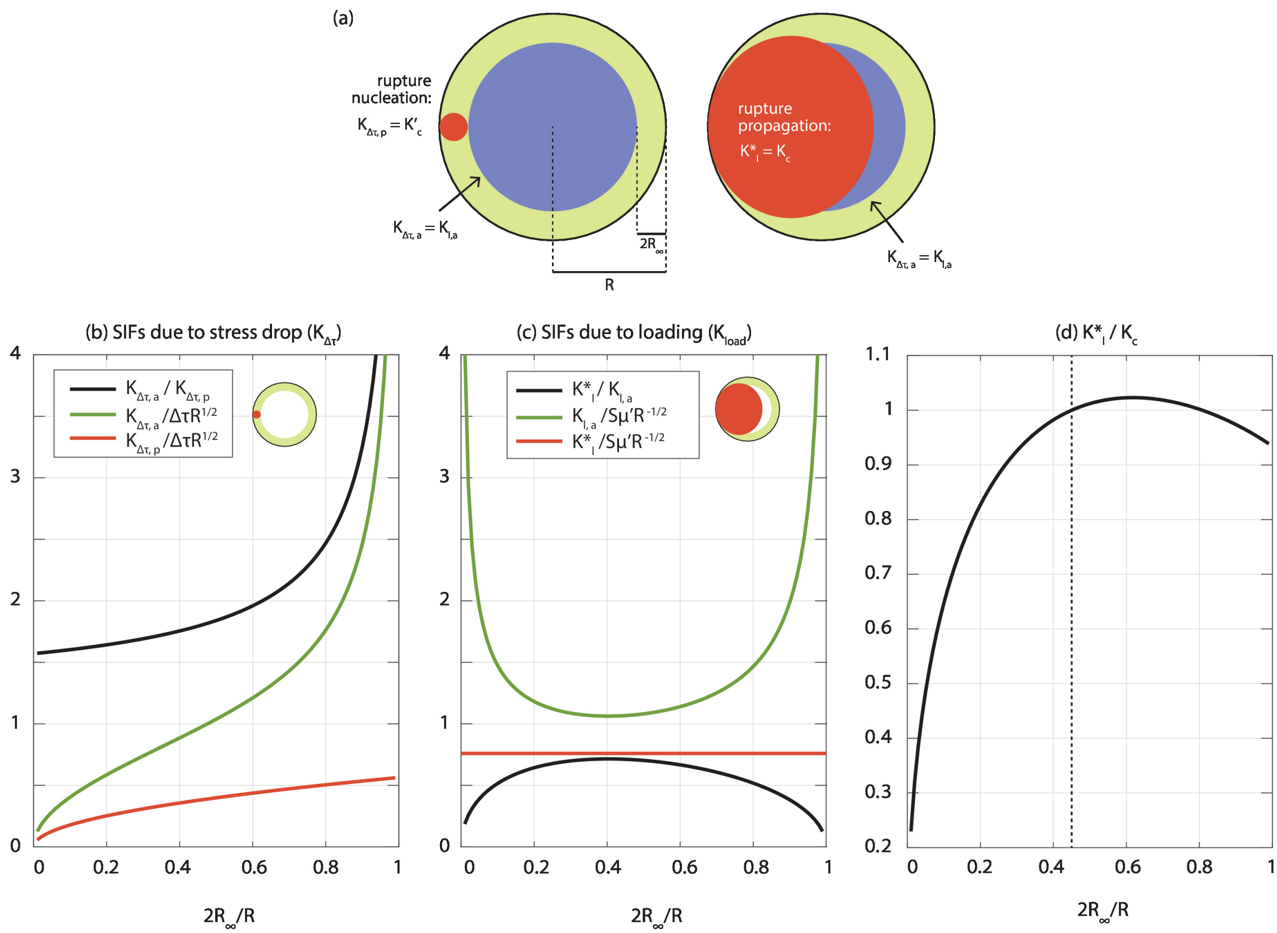

Figure B.3. (a) Summary of the energy balance criteria governing creep propagation (green), rupture nucleation (red, left) and rupture propagation (red, right). (b) Normalized stress intensity factors for constant stress drop crack with an annular and circular shape (shown in the inset), representing the SIF of the creep front and a penny-shaped seismic rupture as it nucleates within the creeping region of the asperity, and their ratio. As expected, the limiting value as $R \gg 2R_\infty$ is the ratio of SIF for a 2-D and a penny shaped crack ($\pi/2$); (c) normalized SIFs related to slip at $r \geq R$, for an annular crack (green), and minimum value during rupture growth, for the rupture history in Fig. B.2 (red). (d) The ratio K_l^*/K_c, from eq. B.11. To the left of the dotted line (large R) partial ruptures are possible.

C: Slip budget

The slip deficit at the time of the first nucleation is given by $v_{pl}T_{nucl}$, and from eq. 13 we have

$$S_{tot} = \begin{cases} \dfrac{4\Delta\tau}{\pi\mu'} R & R < 2R_\infty \\ \\ \dfrac{16\Delta\tau}{\pi\mu'} R_\infty \left(1 - \dfrac{R_\infty}{R}\right) & R \geq 2R_\infty. \end{cases} \tag{C.1}$$

In order to calculate the average slip from the propagation of the creep front, we need to know the slip profile for an annular crack analyzed in section A . While there are simple expressions for this problem for 1D cracks, there are no closed form solutions for the annular crack. Therefore we use the following approximation: points ahead of the creep front don't slip, and points behind it accumulate slip at a constant rate v_{cr} (which, as discussed earlier, is of the order of v_{pl}). At the time of nucleation, the total slip at a point of radius r is $v_{cr}\left(T_{nucl} - t(r)\right)$, where $t(r)$ is the time when the front reached r. Approximating this time by the inverse of eq. A.17, we obtain

$$s_{creep}(r) = \begin{cases} \dfrac{4\Delta\tau}{\pi\mu'} \dfrac{v_{cr}}{v_{pl}} \dfrac{r^2}{R} & R < 2R_\infty \\ \\ \dfrac{4\Delta\tau}{\pi\mu'} \dfrac{v_{cr}}{v_{pl}} \dfrac{r^2 - (R - 2R_\infty)^2}{R} & R \geq 2R_\infty, \end{cases} \tag{C.2}$$

We integrate this expression to obtain the average slip on the asperity at the time of nucleation:

$$S_{creep} = \begin{cases} \dfrac{2\Delta\tau}{\pi\mu'} \dfrac{v_{cr}}{v_{pl}} R & R < 2R_\infty \\ \\ \dfrac{32\Delta\tau}{\pi\mu'} \dfrac{v_{cr}}{v_{pl}} \dfrac{R_\infty^2}{R} \left(1 - \dfrac{R_\infty}{R}\right)^2 & R \geq 2R_\infty. \end{cases} \tag{C.3}$$

To constrain v_{cr}/v_{pl}, we consider the initial phase of the creep front propagation, when the annulus can be treated as a 1D crack. As shown in Fig. C.1, the average slip within a stress free crack driven by a slip boundary condition is the same as that of a linear slip profile given by constant slip rate $v_{cr} = v_{pl}$. However, the (negative) stress drop crack that cancels the stress intensity factor contributes negative slip, equal to half of the average slip for the stress free crack. Therefore we match the correct average slip in the annulus by setting $v_{cr} = v_{pl}/2$; v_{cr} should be thought of as an average slip velocity.

Finally, we consider the slip accumulated during the nucleation phase by treating the nucleating patch as constant stress drop crack of radius R_∞ (cf. section 5). The average slip due

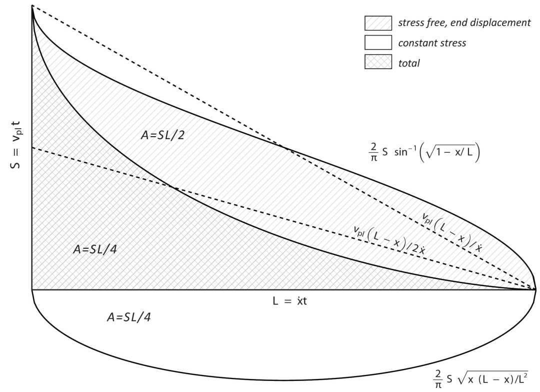

Figure C.1. Slip profile for a stress free crack with a displacement boundary condition; the constant stress drop crack which negates the SIF from the displacement driven crack; and their combination. The dotted lines are the slip profiles assuming $v = 0$ ahead of the crack tip, and $v = v_{cr}$ behind, with $v_{cr} = v_{pl}$ and $v_{cr} = v_{pl}/2$.

to this crack embedded within an asperity of radius R is given by

$$S_{nucl} = \frac{16\Delta\tau}{7\pi\mu'}\frac{R_\infty^3}{R^2} \tag{C.4}$$

Assuming, as done before, that the stress drops during nucleation and creep propagation have the same absolute value, $\Delta\tau$ is the same in eq. C.1, C.3, C.4, and these values differ only by factors containing R and R_∞.

References

Abercrombie, R. E., P. Poli, and S. Bannister (2017), Earthquake directivity, orientation, and stress drop within the subducting plate at the Hikurangi margin, New Zealand, *Journal of Geophysical Research*, doi:10.1002/2017JB014935.

Beeler, N. M., D. L. Lockner, and S. H. Hickman (2001), A simple stick-slip and creep-slip model for repeating earthquakes and its implication for microearthquakes at Parkfield, *Bulletin of the Seismological Society of America*, *91*(6).

Boatwright, J. (2007), The persistence of directivity in small earthquakes, *Bulletin of the Seismological Society of America*, *97*(6), 1850–1861, doi:10.1785/0120050228.

Calderoni, G., A. Rovelli, Y. Ben-Zion, and R. Di Giovambattista (2015), Along-strike rupture directivity of earthquakes of the 2009 L'Aquila, central Italy, seismic sequence, *Geophysical Journal International*, *203*(1), 399–415, doi:10.1093/gji/ggv275.

Chen, K. H., R. M. Nadeau, and R. J. Rau (2007), Towards a universal rule on the recurrence interval scaling of repeating earthquakes?, *Geophysical Research Letters*, *34*(16), doi:10.1029/2007GL030554.

Chen, K. H., R. J. Rau, and J. C. Hu (2009), Variability of repeating earthquake behavior along the Longitudinal Valley fault zone of eastern Taiwan, *Journal of Geophysical Research*, *114*(5), doi:10.1029/2007JB005518.

Chen, T., and N. Lapusta (2009), Scaling of small repeating earthquakes explained by interaction of seismic and aseismic slip in a rate and state fault model, *Journal of Geophysical Research*, *114*, 1–12, doi:10.1029/2008JB005749.

Clements, D. L., and W. T. Ang (1988), Stress intensity factors for the circular annulus crack, *International Journal of Engineering Science*, *26*(4), 325–329, doi:10.1016/0020-7225(88)90112-7.

Dieterich, J. H. (1978), Time-dependent friction and the mechanics of stick-slip, *Pure and Applied Geophysics*, *116*(4-5), 790–806, doi:10.1007/BF00876539.

Dieterich, J. H. (1992), Earthquake nucleation on faults with rate-and state-dependent strength, *Tectonophysics*, *211*(1-4), 115–134, doi:10.1016/0040-1951(92)90055-B.

Eshelby, J. (1957), Determination of the elastic field of an ellipsoidal inclusion, and related problems, *Proceedings of the Royal Society of London*, doi:10.1098/rspa.1957.0133.

Freund, L. B. (1990), *Dynamic Fracture Mechanics*, Cambridge Monographs on Mechanics, doi:DOI:10.1017/CBO9780511546761.

Griffith, A. A. (1921), The phenomena of rupture and flow in solids, *Philosophical Transactions of the Royal Society A: Mathematical, Physical and Engineering Sciences*, *221*(582-593), 163–198, doi:10.1098/rsta.1921.0006.

Hawthorne, J. C., M. Simons, and J. P. Ampuero (2016), Estimates of aseismic slip associated with small earthquakes near San Juan Bautista, CA, *Journal of Geophysical Research*, *121*(11), 8254–8275, doi:10.1002/2016JB013120.

Herrendorfer, R., Y. van Dinther, T. Gerya, and L. A. Dalguer (2015), Earthquake supercycle in subduction zones controlled by the width of the seismogenic zone, *Nature Geosci*, *8*(6), 471–474, doi:10.1038/ngeo2427.

Irwin, G. (1957), Analysis of Stresses and Strains Near the End of a Crack Traversing a Plate, *Journal of Applied Mechanics*, *24*(Sep), 361–364, doi:noDOI.

Kaneko, Y., and P. M. Shearer (2015), Variability of seismic source spectra, estimated stress drop, and radiated energy, derived from cohesive-zone models of symmetrical and asymmetrical circular and elliptical ruptures, *Journal of Geophysical Research B: Solid Earth*, *120*(2), 1053–1079, doi:10.1002/2014JB011642.

Kroupa, F. (1960), Circular edge dislocation loop, *Czechoslovak Journal of Physics*, *10*(4), 284–293, doi:10.1007/BF02033533.

Lapusta, N. (2003), Nucleation and early seismic propagation of small and large events in a crustal earthquake model, *Journal of Geophysical Research*, *108*, 1–18, doi: 10.1029/2001JB000793.

Madariaga, R. (1977), High frequency radiation from crack (stress drop) models of earthquake faulting, *Geophysical Journal of the Royal Astronomical Society*, *51*(3), 625–651, doi:10.1111/j.1365-246X.1977.tb04211.x.

Mavrommatis, A. P., P. Segall, and K. M. Johnson (2017), A physical model for interseismic erosion of locked fault asperities, *Journal of Geophysical Research: Solid Earth*, *122*(10), 8326–8346, doi:10.1002/2017JB014533.

Nadeau, R. M., and L. R. Johnson (1998), Seismological studies at Parkfield VI: Moment release rates and estimates of source parameters for small repeating earthquakes, *Bulletin of the Seismological Society of America*, *88*(3).

Rice, J. (1989), Weight function theory for three-dimensional elastic crack analysis, in *Fracture Mechanics: Perspectives and Directions (Twentieth Symposium), STP18819S, ASTM International*, pp. 29–57.

Rice, J. R. (1993), Spatio-temporal complexity of slip on a fault, *Journal of Geophysical Research*, *98*(B6), 9885, doi:10.1029/93JB00191.

Rubin, A. M., and J. Ampuero (2005), Earthquake nucleation on (aging) rate and state faults, *Journal of Geophysical Research*, *110*(2), 1–24, doi:10.1029/2005JB003686.

Ruina, A. (1983), Slip instability and state variable friction law, *J. Geophys. Res.*, *88*, 10,359–10,370, doi:10.1029/JB088iB12p10359.

Sammis, C. G., and J. R. Rice (2001), Repeating earthquakes as low-stress-drop events at a border etween locked and creeping fault patches, *Bulletin of the Seismological Society of America*, *91*(3), 532–537, doi:10.1785/0120000075.

Sato, T., and T. Hirasawa (1973), Body wave spectra from propagating shear cracks, *Journal of Physics of the Earth*, *21*, 415–431, doi:10.4294/jpe1952.21.415.

Segall, P. (2010), *Earthquake and Volcano deformation*, 517 pp., doi:10.1002/0471743984.vse7429.

Segall, P., and A. M. Bradley (2012), Slow-slip evolves into megathrust earthquakes in 2D numerical simulations, *Geophys. Res. Lett.*, *39*, 2–6, doi:10.1029/2012GL052811.

Selvadurai, A. P. S., and B. M. Singh (1986), The axial displacement of a disc inclusion embedded in a penny-shaped crack, *ZAMP Zeitschrift fuer angewandte Mathematik und Physik*, *37*(1), 64–77, doi:10.1007/BF00955519.

Sih, G. C. (1973), *Handbook of Stress-intensity Factors*, Bethlehem, Pa., Lehigh University.

Tada, H., P. C. Paris, and G. R. Irwin (2000), *The Stress Analysis of Cracks Handbook*, 58 pp., Del Research Corp, Hellertown PA, doi:10.1115/1.801535.

Uchida, N., T. Matsuzawa, W. L. Ellsworth, K. Imanishi, T. Okada, and A. Hasegawa (2007), Source parameters of a M4.8 and its accompanying repeating earthquakes off Kamaishi, NE Japan: Implications for the hierarchical structure of asperities and earthquake cycle, *Geophysical Research Letters*, *34*(20), doi:10.1029/2007GL031263.

Uchida, N., T. Matsuzawa, W. L. Ellsworth, K. Imanishi, K. Shimamura, and A. Hasegawa (2012), Source parameters of microearthquakes on an interplate asperity off Kamaishi, NE Japan over two earthquake cycles, *Geophysical Journal International*, *189*(2), 999–1014, doi:10.1111/j.1365-246X.2012.05377.x.

Wang, X., S. B. Lambert, and G. Glinka (1998), Approximate weight functions for embedded elliptical cracks, *Engineering Fracture Mechanics*, *59*(3), 381–392, doi:10.1016/S0013-7944(97)00139-2.

Werner, M., and A. Rubin (2013), Mechanical Erosion of the Seismogenic Zone by Creep from below on Rate-and-State Faults, in *AGU Fall Meeting Abstracts*, San Francisco.